20

Transient Heat Transfer and Energy Transport in Packed Bed Thermal Storage Systems

Pei Wen Li[1], Jon Van Lew[1], Wafaa Karaki[1],
Cho Lik Chan[1], Jake Stephens[2] and James. E. O'Brien[3]
[1]*Department of Aerospace and Mechanical Engineering*
The University of Arizona, Tucson, AZ 85721,
[2]*US Solar Holdings LLC., 1000 E. Water Street, Tucson, AZ 85719,*
[3]*Idaho National Laboratory, Idaho Falls, Idaho 83415,*
USA

1. Introduction

Compared to fossil fuel energy resources, the major types of renewable energy—such as wind power, solar energy, ocean currents, and tidal energy—generally possess the innate characteristics of intermittence of availability, fluctuation of magnitude, as well as low energy density (Li, 2008). However, the utilization of energy and power in industry, living, and working often requires high energy densities, and demand may be out of phase with the period of availability of renewable energy. In other words, renewable energy is not always load following. This variability creates a demand for energy storage when people develop renewable energy technologies (Kolb, 1998).

Among the several types of renewable energy, solar energy has the largest proportion of the total available and may be directly used as thermal energy in conventional thermal power plants, or converted into electrical power directly using photovoltaic panels. Although direct electrical energy storage in batteries or capacitors may have a high efficiency, it is still very challenging and expensive—particularly when storing a large quantity of electrical energy (Spiers, 1995). Electricity may be indirectly stored by pumping water to reservoirs, or by compressing air, or by electrolyzing water and making hydrogen fuel, etc. However, these methods often have low round-trip efficiency (from electricity to electricity), or are restricted by the availability of geographical conditions or suitable locations. In comparison, it has been recognized that direct solar thermal energy storage is relatively easy to approach at a reasonably low cost and high efficiency, and the energy storage capacity can be much larger than that of direct electricity storage (Price et al., 2002; Montes et al, 2009). Thermal energy storage systems use materials that can be kept at high temperatures in insulated containers. The heat retrieved can then be used in conventional thermal power plants for power generation at times when sunlight is not available or when weather conditions are not favorable (Singer et al, 2010; Laing et al, 2010).

Researchers worldwide have done a great amount of research and development on concentrated solar thermal power generation technologies in the last ten years (Renewable Energy Policy Network for the 21st Century, 2007). Particularly, with these efforts solar trough and solar tower concentrated thermal power generation technologies have become more and more reliable and matured, and the cost of concentrated solar power systems have been significantly reduced due to increased productivity and demand (Pitz-Paal et al., 2007; Herrmann & Kearney, 2002; Gil et al., 2010.).

It has been widely recognized that further cost reduction of electricity generation using concentrated solar thermal power may be accomplished by adding solar thermal storage systems. Storage provides the heat necessary for operation of thermal power plants when sunlight availability is out of phase, and thus increases the operational capacity (in terms of the daily operational time) of the power plants. In addition, the extended operation of solar thermal power plants using stored thermal energy can significantly improve the power dispatch ability (Herrmann & Kearney, 2002) of the power plant.

Other than electrical power generation, solar thermal energy can also be stored for sundry applications such as house heating, hot water supply, industrial drying processes, as well as heating for greenhouse agriculture and animal husbandry. From an energy efficiency perspective, direct use of solar thermal energy for heating is much more efficient than using electricity for heating, as electricity generation requires much more input of other types of energy than the generated electricity. Therefore, although thermal energy storage is not a new technology, it will receive more and more attention, particularly with the development of renewable energy technologies.

2. Brief review of thermal storage techniques

The ideal scenario for thermal energy storage is such that the energy-carrying fluid is stored in a thermal storage system and can be withdrawn at a temperature of no degradation from that of when the fluid was stored. On the basis of this fundamental distinction, one may classify thermal energy storage systems into two categories: (1) a system with direct storage of heat transport fluid, which may approach the performance of an ideal thermal storage system; (2) two-medium heat storage system, which has a fluid serving as heat- carrying medium, and another medium, either solid materials or a liquid, serving the purpose as of a primary thermal storage material. A two-medium heat storage system uses a reduced amount of expensive heat transfer fluid while sacrificing the energy storage efficiency.

A first generation direct heat transfer fluid storage system usually has two storage tanks, as shown in Fig. 1(a), one for hot fluid and the other for cold fluid (Herrmann at al., 2004). During the energy storage process, fluid from the cold tank is pumped to the solar field to be heated and then stored in the hot fluid tank; while during the energy discharging process, fluid from the hot fluid tank is pumped out to release heat to the power plant and afterwards, flows back to the cold fluid tank. Although there are two tanks in such a thermal storage system, the heat transfer fluid only occupies a volume equivalent to that of one tank at any instant in time. This means that the elimination of one tank in the system is possible. As a consequence, a second generation direct heat transfer fluid storage system has only one tank, as shown in Fig. 1(b). A stratification of fluid, which maintains hot fluid on top of cold fluid, is important to such a single tank thermal storage system (Michel et al., 2009; Abdoly & Rapp, 1982; Krane R.J. & Krane M.J.M., 1992; Brosseau et al., 2005). During a heat charging

process, hot fluid is injected from the top of the tank, whereas cold fluid is pumped out from bottom of the tank. The opposite is true for the heat discharge process, during which hot fluid is pumped out from top of the tank and cold fluid is injected into the tank from the bottom (Canada et al., 2006).

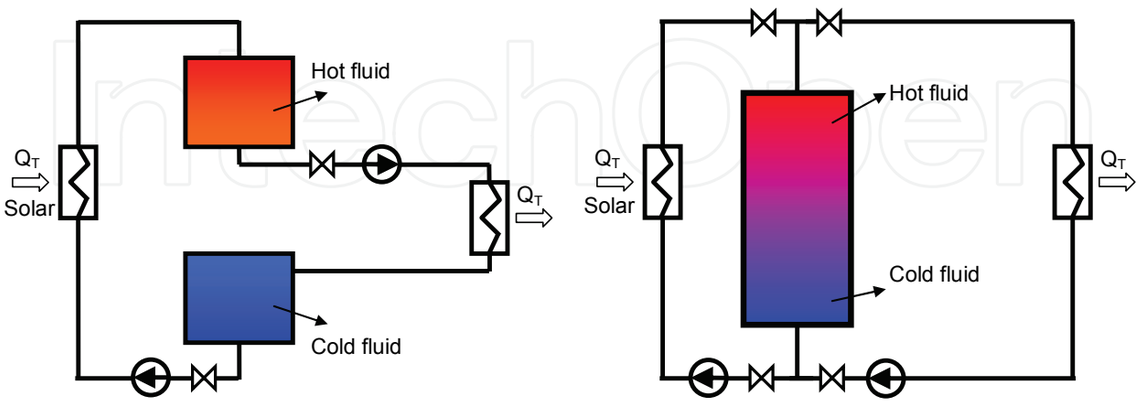

(a) (b)

Fig. 1. Thermal storage using heat transport fluid only

Two-medium heat storage systems must have a heat transport fluid and a primary thermal storage material (Laing et al, 2006), either solid or liquid. Also, a two-medium heat storage system typically uses only a single tank. Depending on the contact and heat transfer interaction between the heat-carrying fluid and the primary energy storage material, the storage system may have two types. The first type, as shown in Fig. 2(a), is one that includes loosely packed solid materials (such as rocks, pebbles of metals, and capsules of phase change materials (PCM), etc.) as a porous bed held in a container and through which the heat transport fluid (HTF) flows and transports energy to or from the solid material. In this type of thermal storage system, the heat transfer between thermal storage material and the heat transport fluid is relatively efficient due to the ubiquitous contact between the fluid and storage materials. The second type of two-medium heat storage system, as shown in Fig. 2(b), is such that the heat transfer fluid flows in tubes or pipes that run through thermal storage material, either solid (such as, concrete, wax, sands, soil (Nassar et al., 2006), salts, etc), or liquid (such as oil, or liquid salts, etc). Due to the smaller contact area between the fluid and thermal storage material, the heat transfer between the fluid and the thermal storage material in this case is worse compared to that of the first type.

Cost-effectiveness is always the dictating criterion for selecting a thermal storage system for a specific application. However, there are many factors that can influence the cost of a thermal storage system; for example, the cost of the heat transfer fluid is a key factor which can determine whether a direct HTF storage system or a two-medium thermal storage should be used. A high-pressure tank may be needed if the vapor pressure of the heat transfer fluid is high, or a stainless steel tank may be needed to mitigate corrosion problems. Possible chemical interaction between tank material, the heat transfer fluid, and primary thermal storage material, if applicable, must also be prevented.

The following section provides a survey of suitable heat transport fluids and solid materials for thermal energy storage applications.

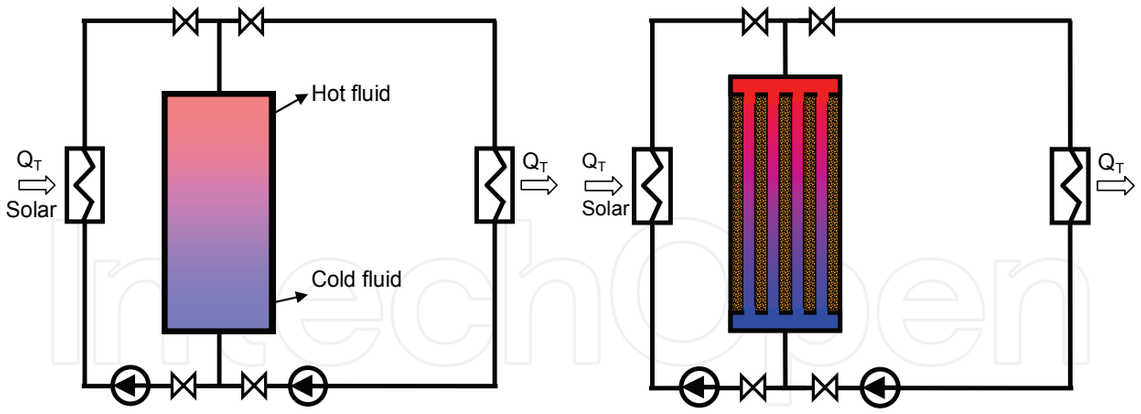

(a) direct contact heat transfer (b) heat transfer through fluid pipes

Fig. 2. Thermal storage using a primary thermal storage material with heat transport fluid

3. Thermal storage materials and heat transfer fluids

The quantity of sensible thermal energy stored in a mass is given by the equation:

$$Q_T = V \rho C(T_H - T_L) \tag{1}$$

where V, ρ, and C are the volume of the mass, the average density of the mass, and the heat capacity of the material, respectively.

Obviously, a high specific heat and a large density are both important for a substance to be a good thermal energy storage material, for that will keep the volume of the storage container small. Other required properties such as high thermal conductivity, low cost, low thermal expansion coefficient, etc. are also important. For a liquid to serve as a heat transport fluid or a thermal storage material, a low solidification point, high boiling point, and low vapor pressure, are all important. Particularly, if the vapor pressure is high, it will require pressurized storage tanks, which can significantly increase the cost of the thermal storage system.

3.1 Properties of solid thermal storage materials

Solid materials, suck as concrete (Zhang et al., 2004), sand, rock, brick, soil, graphite, silicon carbide, taconite, cast iron, and even waste metal chips, have been considered or applied for thermal energy storage purposes. Depending on the formation and granular size of these solid materials, some of them can be used to form a packed bed storage system as illustrated in Fig. 2(a) and others may only be suitable for use in a storage system as shown in Fig. 2(b). The main properties of some of these materials (Tritt, 2005; Hasnain, 1998) are given in Table 1.

Compared to sensible heat storage, the high latent heat associated with phase change of a material offers the potential for higher energy storage densities. There are two approaches using phase change material (PCM) for thermal storage. One is encapsulation of small amounts of PCM in spherical or cylindrical capsules (Wu et al., 2011), which can be arranged to form a packed bed. Heat transport fluid can flow through the packed bed for energy delivery and extraction. This approach needs encapsulation technologies, either coating or canning. The other approach is to embed the PCM in a matrix made of another solid material with high heat conduction, and HTF pipes run through the PCM matrix (Sari

& Kaygusuz, 2001; Regin et al., 2008). The use of a matrix material (e.g. graphite or metal mesh) helps enhance heat conduction in the PCM.

Medium	melting(°C) (or crumbles)	ρ (kg/m^3)	C(kJ/kg·°C)	ρ·C(kJ/m^3·°C)	k(W/m·°C)
Aluminum	660	2700	0.92	2484.0	250
Brick (common)	1800	1920	1.0	1920.0	1.04
Fireclay	1800	2100-2600	1.0	2100-2600	1-1.5
Soil (dry)	1650	1200-1600	1.26	1512-2016	1.5
Granite	1215	2400	0.79	1896	1.7-4.0
Sand (dry)	1500	1555	0.8	1244	0.15-0.25
Sandstone	1300	2000-2600	0.92	1840-2392	2.4
Rocks	1800	2480	0.84	2086.6	2-7
Concrete	1000 (Crumbles)	2240-2400	0.75	1680-1800	1.7
Graphite	3500	2300-2700	0.71	1633-1917	85
Silicon carbide	2730	3210	0.75	2407.5	3.6
Taconite	1538	3200	0.8	2560	1.0-2.0
Cast iron	1150	7200	0.54	3888	42-55

Table 1. Properties of solid material suitable for thermal energy storage application

There are many suitable PCM for relatively high temperature thermal storage purposes, with melting temperatures ranging from below 100 Celsius up to several hundred Celsius. Paraffin is a typical PCM used for low-grade heat storage. For concentrated high temperature solar thermal energy storage, alloy and molten salts are often considered. Table 2 includes the properties of some alloys and salts (Zalba et al., 2003).

Medium	ρ kg/m^3	Heat of fusion (kJ/kg)	Melting temperature (°C)
Mg/Cu/Ca (52/25/23)	2000	184	453
Mg/Cu/Zn (60/25/15)	2800	254	452
Al/Cu/Mg/Zn (54/22/18/6)	3140	305	520
Al/Mg/Zn (59/35/6)	2380	310	443
Al/Cu/Si (65/30/5)	2730	422	571
$NaNO_3$	2260	172	307
KNO_3	2110	266	333
K_2CO_3/Na_2CO_3(51/49)	2400	163	710
CaCl/NaCl(67/33)	2160	281	500

Table 2. Properties of alloy and salt PCM for thermal energy storage application

3.2 Heat transfer fluids for thermal storage application

Heat transport fluid (HTF), either used for direct fluid storage or as a heat-carrying medium, must have favorable properties for heat transfer and at the same time, must be stable and have a low vapor pressure. Molten salts and oils are the two major types of heat transport fluids developed so far.

Most molten salts have low vapor pressures, which is an advantage to the large quantity storage of thermal energy as no pressurized tanks are needed. However, many molten salts

freeze at relatively high temperatures (in the range of 120 °C to 250 °C), which can cause severe problems if freezing or solidification occurs in a solar heat collection system. There has been some research done worldwide to develop eutectic salt mixtures to lower the freezing points of salts. If the freezing points of salts are reduced to about 100 °C the freezing problem is expected to be much more manageable. Table 3 lists the properties of some typical eutectic molten salts popular in concentrated solar thermal power plant applications (Bradshaw & Siegel, 2009).

Medium (Company)	Components	Freezing/Maximum °C
Hitec XL (Costal Chemical)	$NaNO_3$ +KNO_3 +$Ca(NO_3)_2$	140/500
Hitec (Same as above)	$NaNO_3$ +KNO_3 +$NaN\ O_2$	142/538
Hitec Solar Salt (Same as above)	$NaNO_3$ +KNO_3	240/593

Table 3. Molten salts suitable as heat transfer fluids

Mineral oils, or synthetic oils, are popular HTFs in trough concentrated solar thermal power plants. For large quantity thermal storage large containers are used. If the vapor pressure of oil is high, vessels for thermal energy storage must withstand high pressure, which can dramatically drive the cost up. Therefore, synthetic oil or mineral oil is usually used as HTF but not for fluid that flows through heat storage system (Becker, 1980). Table 4 lists several mineral oils and synthetic oils which are tipically used as HTF for concentrated solar thermal power application (Therminol VP-1, 1999; Produc resources, Radco).

Medium (Company)	Components	Maximum/boiling °C
Xceltherm® series (Radco Industries, Inc)	Synthetic oil	~310
Therminol® series (Solutia)	synthetic oil	~400

Table 4. Major synthetic oils suitable for HTF in concentrated solar thermal power plant

4. Model of an ideal thermal energy storage system

In an ideal thermal storage system high temperature heat transfer fluid is stored, and when it is withdrawn, there should be no temperature degradation. Such a system requires that there be no heat loss and no heat transfer when the HTF is stored in or withdrawn from a tank.

Contingent upon the thermal insulation being perfectly maintained, the two-tank heat transfer fluid storage system in Fig. 1(a) can operate like an ideal thermal energy storage system. It has been discussed before that a two-tank storage system can be replaced by a single tank storage system as shown in Fig. 1(b), in which a stratification of fluid (hot on top of cold), or a thermocline mechanism, must be maintained. However, even if the thermocline is maintained, the heat conduction between hot fluid and cold fluid may cause a temperature drop in the hot fluid, which will not allow for ideal thermal storage performance in such a system. A modification proposed by the current authors (Van Lew et al., 2009) used a thermal insulation baffle in the single tank, which separates the hot fluid from the cold fluid, as shown in Fig. 3. In this system, if the floating thermal insulation baffle prevents heat conduction from the hot fluid to the cold fluid, an ideal thermal storage performance can be achieved. In respect to both the cost reduction and energy storage performance, the single tank with floating thermal insulation baffle will be the ideal thermal storage system considered in this book chapter.

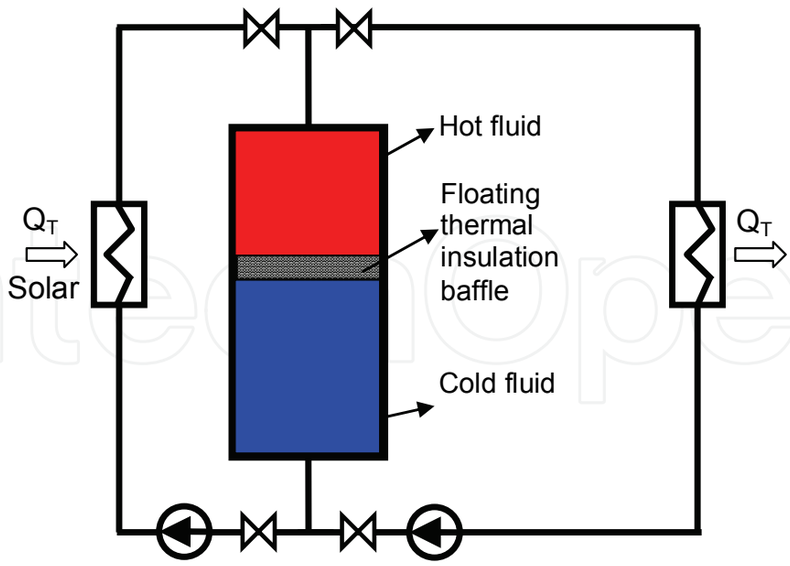

Fig. 3. Schematic illustration of a single tank ideal thermal storage system

Whereas physically an ideal thermal storage system has the clearly identifiable features previously detailed, mathematically it should be described as a system that has an energy storage efficiency of 1.0. With this in mind, the following definition of thermal energy delivery efficiency is adopted for thermal energy storage systems:

$$\eta = \frac{\int_0^{t_{ref,discharge}} [T_{f(z=H,t)} - T_L]dt}{(T_H - T_L) \cdot t_{ref,discharge}} \tag{2}$$

where z is the vertical coordinate of the tank and H is the height of the tank. For adopting this definition, we assume that the average heat capacity, Cp , and the mass flow rates of the heat transfer fluid for the charging and discharging processes are the same. The integration on the numerator of Eq. (2) is the energy discharge in an actual process, and the value on the denominator is the ideal energy discharge.

For the ideal thermal storage system, it is assumed that the temperature of the hot fluid in a charging process is kept constant at T_H ; and in the discharging process the discharged fluid keeps a constant temperature of T_H as well. After releasing heat in a heat exchanger, the fluid returns to the bottom of the storage tank at a constant temperature, T_L . To substitute these conditions from the ideal thermal storage system into Eq(2), the fluid temperature $T_{f(z=H,t)}$ during the discharge process in a time period of 0 to $t_{ref,discharge}$ should be equal to the high temperature, T_H . This will make the energy delivery efficiency equal to $\eta = 1.0$ for the ideal thermal storage system.

In a real thermal energy storage system, such as the systems shown in Fig. 2, it is easy to understand that when cold fluid is pumped into the tank from the bottom, it will extract heat from the solid thermal storage material and be warmed up when it flows out of the tank. However, after a certain time, the cold fluid going into the tank may not be heated up sufficiently before it flows out from top of the tank. Unfortunately, this temperature

degradation is inevitable due to the heat transfer between the solid thermal storage material and the heat transfer fluid, even if initially the solid thermal storage material is fully charged, or its temperature is exactly equal to T_H.

Considering the need of heat transfer fluid in a power plant, it is always important that during the required operational period of time, $t_{ref,discharge}$, the temperature of the heat transfer fluid have minimum or no degradation from the temperature the fluid is stored at. To meet this requirement in an actual thermocline storage system, one needs to first store a sufficient amount of energy (more than the ideal amount) in the tank. This requires a storage tank to have a sufficiently large thermal energy storage capacity as well as a sufficiently long charge time that allows heat to be charged to the tank. Giving this requirement as a mathematical expression,it is such that:

$$\left\{\left[\rho_s C_s(1-\varepsilon)+\rho_f C_f \varepsilon\right]V_{real}\right\} > \left[\left(\rho_f C_f\right)V_{ideal}\right] \tag{3}$$

In engineering reality, one needs to know, specifically, how large the real thermal storage volume, V_{real}, is and how long a charging time is necessary, if the assumed operation time period of a power plant is $t_{ref,discharge}$. This must be addressed through mathematical analysis.

In the following section, the modeling of the heat transfer and energy transport between the solar thermal storage material and the heat transfer fluid will be described. The goal of the modeling analysis is to predict the size of the storage tank and the period of time required to charge the tank for a given subsequent period of heat discharge from the system, within which minimum or no temperature degradation must be maintained.

5. Analysis of transient heat transfer and energy transport in a packed bed

5.1 Thermal storage/delivery process explained

The following qualitative analysis helps readers better understand the behavior of the fluid temperature variation from a thermocline tank during a discharging operation. When a tank of volume V_{ideal} is filled with thermal storage material at a void fraction of ε, the volume for heat transfer fluid in the tank will be εV_{ideal}, and the volume of the primary thermal storage material must be the remaining portion, $(1-\varepsilon)V_{ideal}$. Due to the existence of solid filler material in the tank, the heat transfer fluid velocity in the charge/discharge processes is higher than that in an ideal thermocline tank as the same mass flow rate of heat transfer fluid is considered. The mass flow rate is a condition determined by the required power output of the power plant, regardless of what type of thermal storage system is used.

Assume that a thermocline tank is initially fully charged. During a thermal discharge process the temperature of the fluid flowing out from top will decrease after a time when the pre-existing hot fluid in the tank is completely discharged; from then on, the hot fluid discharged out from the top is originated from cold fluid that picks up energy from the solid material during the discharging process. The longer the discharge process progresses, the more the temperature of the discharged fluid will decrease. This scenario is illustrated in Fig. 4.

In order to avoid the temperature degradation as show in Fig. 4, one either needs to use an ideal thermal storage system or to have a thermocline system that stores much more energy than is needed so that during the required time period, $t_{ref,discharge}$, the temperature degradation of the discharged fluid is minimal or ignorable.

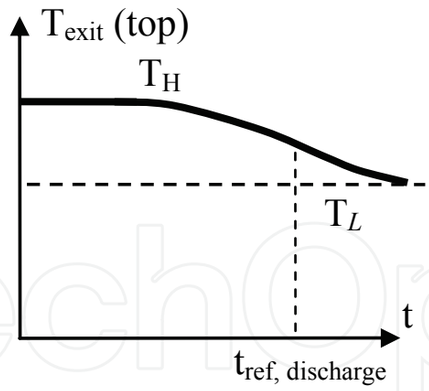

Fig. 4. The temperature variation of heat transfer fluid during discharge from a tank having filler material

5.2 A generalized mathematical modeling

In general, the thermocline thermal storage systems shown in Fig. 2(a) and 2(b) can be regarded as systems that have porous medium, through which a fluid flows and heat transfer between the solid and fluid occurs. Therefore, generalized governing equations for the energy balance in the solid material and fluid can be constructed. As a representative case of a tank filled with porous medium, the system shown in Fig. 2(a) is subjected to analysis for the objective of formulating an analytical model.

Shown in Fig. 5 is a one-dimensional control volume of an element *dz* in the packed bed. For convenience in analysis, the positive direction of coordinate z is set to be always identical to the fluid flow direction. In the energy charge process hot fluid flows into the tank from the top, and thus $z = 0$ is at the top of the tank. During heat discharge process, cold fluid flows into the tank from bottom to extract heat from the solid material, and this makes $z = 0$ at the bottom of the tank.

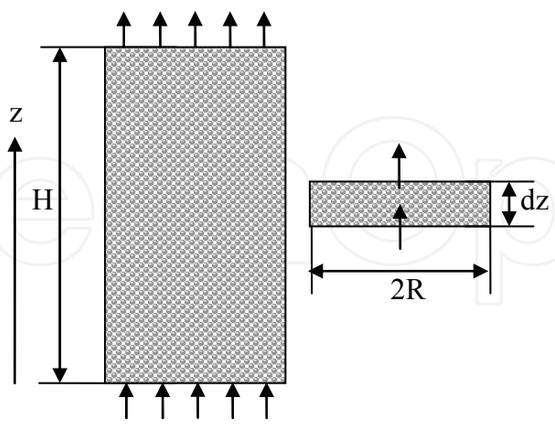

Fig. 5. Schematic of a packed-bed thermal storage system and a control volume for analysis

Several modeling assumptions are made to reasonably simplify the analysis of heat transfer between the heat transfer fluid and the solid packing material:

1. There is a uniform radial distribution of fluid flow and filler material throughout the storage tank. This allows the model to be one-dimensional, only in the z direction.

2. Assume that the particles of filler material have only point contact and therefore axial heat conduction between layers of filler material is negligible.
3. Heat conduction in the axial direction in the fluid is negligible compared to the convective heat transfer.
4. The lumped heat capacitance method is applied to the transient heat conduction in the filler material (particles of size of 0.25-5.0 cm in nominal diameter). When this method is inadequate, due to the large size of solid filler material, a modified lumped capacitance method will be used, which introduces a modified heat transfer coefficient for the convection heat transfer between the fluid and the solid filler material.
5. Assume that there is no heat loss from the storage tank to the surroundings. This assumption applies to both the processes of energy charge and discharge, as well as the resting time between a charge and a discharge.

Assumption (3) is valid when the Peclet number (=RePr) in the HTF is sufficiently large, which is satisfied for most thermal energy storage applications (Kays, 2005). Assumption (4) is valid when the Biot number $(=hL_p / k_s)$ for the thermal storage material is sufficiently small (Incropera, 2002). If the Biot number is large, a correction to the heat transfer accounting for the effects of an internal temperature gradient in the filler material will be considered. Heat loss from a thermal storage tank is inevitable and should be considered. However, from the design point of view, one needs to first decide on the dimensions of a storage tank in order to find the heat loss. To compensate for the heat loss from the tank, a larger volume heat storage tank and a longer heat charge period may be adopted. A simple way of refining this design is to increase both the heat charge time and tank size with a factor that is equal to the ratio of heat loss versus the projected heat delivery. To focus on the main issues, the current work determines the dimensions of a storage tank without considering heat loss. The assumption of no heat loss to the surroundings also provides a basis for using the results from a heat charge process as the initial condition of the following discharge process, and visa versa. By using the end results of one process as the initial conditions of the following process, multiple cyclic energy charges and discharges in the actual operation can be simulated relatively easily.

5.2.1 Energy balance in the heat transfer fluid

Based upon the above modeling assumption (1), the cross-sectional area of the tank seen by the fluid flow is assumed constant at all locations along the axis of the tank, which gives:

$$a_f = \varepsilon \pi R^2 \tag{4}$$

The thermal energy balance of the fluid in the control volume dz is:

$$\rho_f \varepsilon \pi R^2 U(\hbar_z - \hbar_{z+dz}) + hS_s(T_s - T_f)dz = \rho_f C_f \varepsilon \pi R^2 dz \frac{\partial T_f}{\partial t} \tag{5}$$

where the parameter S_s denotes the heat transfer surface area between the filler material and the heat transfer fluid per unit length of the tank; U is the actual fluid velocity in the packed bed:

$$U = \frac{\dot{m}}{\rho_f a_f} \tag{6}$$

The heat transfer coefficient h in Eq. (5) is for the convection between the heat transfer fluid and the packing material. It can be different depending on the flow, packing condition of thermal storage material, fluid properties, and the interaction between packed material and heat transfer fluid, such as is shown in Fig. 2(a) and 2(b). Detailed discussions of S_s and h will be presented following the modeling work.

Using the definition of enthalpy change and a Taylor's series expansion, $\hbar_{z+dz} - \hbar_z = C_f(\partial T_f / \partial z)dz$, the energy balance equation for the heat transfer fluid becomes:

$$\frac{hS_s}{\rho_f C_f \varepsilon \pi R^2}(T_s - T_f) = \frac{\partial T_f}{\partial t} + U\frac{\partial T_f}{\partial z} \tag{7}$$

Introducing the following dimensionless variables,

$$\theta_f = (T_f - T_L)/(T_H - T_L) \tag{8.a}$$

$$\theta_s = (T_s - T_L)/(T_H - T_L) \tag{8.b}$$

$$z^* = z / H \tag{8.c}$$

$$t^* = t / (H / U) \tag{8.d}$$

The dimensionless governing equation for the heat transfer fluid is finally reduced to:

$$\frac{\partial \theta_f}{\partial t^*} + \frac{\partial \theta_f}{\partial z^*} = \frac{1}{\tau_r}(\theta_s - \theta_f) \tag{9}$$

where

$$\tau_r = \frac{U}{H}\frac{\rho_f C_f \varepsilon \pi R^2}{hS_s} = \frac{C_f \dot{m}}{H h S_s} \tag{10}$$

The boundary condition for Eq. (9) is from the fluid inlet temperature, while the initial condition is the temperature distribution in a tank before a charge or a discharge starts.

5.2.2 Energy balance in solid thermal storage material

For the energy balance of the filler material in a control volume *dz* as shown in Fig. 5, it is understood that the filler material delivers or takes heat to or from the passing fluid at the cost of a change in the internal energy of the filler. The energy balance equation is:

$$hS_s(T_s - T_f)dz = -\rho_s C_s(1-\varepsilon)\pi R^2 dz\frac{\partial T_s}{\partial t} \tag{11}$$

By substituting in the dimensionless variables given in Eq. (8), the above governing equation for filler material is reduced to:

$$\frac{\partial \theta_s}{\partial t^*} = -\frac{H_{CR}}{\tau_r}(\theta_s - \theta_f) \tag{12}$$

where

$$H_{CR} = \frac{\rho_f C_f \varepsilon}{\rho_s C_s (1-\varepsilon)} \tag{13}$$

In the energy charge and discharge processes, the filler material and heat transfer fluid will have a temperature difference at any local location. Once the fluid comes to rest upon the completion of a charge or discharge process, the fluid will equilibrate with the local filler material to reach the same temperature, T_{final}. The energy balance of this situation at a local location is:

$$\varepsilon\rho_f C_f T_{f-initial} + (1-\varepsilon)\rho_s C_s T_{s-initial} = \varepsilon\rho_f C_f T_{final} + (1-\varepsilon)\rho_s C_s T_{final} \tag{14}$$

Here, the initial temperatures of primary thermal storage material and HTF are from the results of their respective charge or discharge processes. The final temperatures of the storage material and the fluid are the same after their thermal equilibrium is reached.
According to the assumption of no heat loss from the storage tank, it can be seen that the equilibrium temperature at the end of one process (charge or discharge) will necessarily be the initial condition of the next process in the cycle. This connects the discharge and charge processes so that overall periodic results can be obtained.
The initial temperatures of filler material and fluid in the storage tank should be known. Also, the inlet fluid temperature is known as a basic boundary condition, with which the filler temperature at inlet location z=0 can be easily solved mathematically from Eq. (12).

5.2.3 Energy delivery efficiency

With the solution of the governing equations for filler material and HTF, the discharged fluid temperature from a storage tank can be obtained. With the required heat discharge period being given as $t_{ref,discharge}$, an energy delivery effectiveness can be obtained from Eq.(2) as discussed before. For convenience of expression, the dimensionless form of the required time period of energy discharge is defined as:

$$\Pi_d = \frac{t_{\text{ref,discharge}}}{H/U} \tag{15}$$

Similarly, a dimensionless form of the time period of energy charge is defined as:

$$\Pi_c = \frac{t_{\text{charge}}}{H/U} \tag{16}$$

Substituting the dimensionless energy discharge period Π_d into Eq. (2), we obtain:

$$\eta = \frac{1}{\Pi_d} \int_0^{\Pi_d} \theta_{f(z^*=1,t^*)} dt^* \tag{17}$$

The energy discharge efficiency will obviously be affected by how much energy is charged into the storage tank. Therefore, it should be noted that η is essentially the function of the following four parameters— Π_c / Π_d, Π_d, τ_r, and H_{CR}. By specifying the dimensionless

time period of the discharge process and the mass flow rate, the dimensionless time period of the energy charge can be determined to achieve the objective value of η, which is always desired to approach as close as possible to 1.0.

As has been discussed, a longer energy charging time than energy discharging time is needed in order to achieve an energy delivery effectiveness of approximately 1.0 in a packed-bed system. In addition, the energy storage capacity of a packed-bed tank must be larger than that of an ideal thermal storage tank, as expressed in Eq. (3).

5.2.4 Heat transfer area S_s and heat transfer coefficient h in different types of storage systems

As has been discussed above, the governing equations for the temperatures and energy exchange between the primary thermal storage material and the HTF are generally the same for all the thermal storage systems as schematically shown in Fig. 2. However, the heat transfer coefficients and the heat transfer area between the primary thermal storage material and HTF for different types of storage systems (for example, in Fig. 2(a) and Fig. 2(b)) can be significantly different.

If we consider the use of rocks as a filler material, the heat transfer area between rocks and fluid per unit length of tank was denoted as S_s. Therefore, the unit of S_s is in meters. For spherical filler materials, S_s is obtained through the following steps:

1. The volume of filler material in a unit length Δz of tank is given as $\pi R^2 \Delta z(1-\varepsilon)$.

One sphere of rock has a volume of $V_{sphere} = 4\pi r^3 / 3$, and therefore, in the length of Δz in the tank, the number of rocks is $\pi R^2 \Delta z(1-\varepsilon) / V_{sphere}$. The total surface area of rocks is then determined to be $\pi R^2 \Delta z(1-\varepsilon) \times 4\pi r^2 / V_{sphere}$, which becomes $3\pi R^2(1-\varepsilon)\Delta z / r$ after V_{sphere} being substituted in.

2. Finally, the heat transfer area of rocks per unit length of tank is:

$$S_s = 3\pi R^2(1-\varepsilon) / r \tag{18}$$

The above discussion considers the actual volume (assuming ε is known) for solid 'spherical particles' in a packed volume. Depending on the packing scheme, the void fraction ε in a packed bed with spheres of a fixed diameter may range from 0.26 to 0.476 (Conway & Sloane, 1998). The loosest packaging of spherical rocks in a volume is given by the case where each sphere (of diameter 2*r*) is packed into a cube with side lengths of 2*r*. The densest packing of spheres causes a void fraction of 0.26, which was due to Kepler's conjecture (Hales, 2006). Nevertheless, if the packed bed void fraction ε is known, Eq. (18) should be used for finding S_s.

The heat transfer coefficient h(W/m² °C) between the primary thermal storage material (porous media) and HTF can be found from reference (Nellis & Klein, 2009):

$$h = 0.191 \frac{\dot{m} C_f}{\varepsilon \pi R^2} \mathrm{Re}^{-0.278} \mathrm{Pr}^{-2/3} \tag{19}$$

where *Re* is Reynolds number (equal to $4G\, r_{char} / \mu_f$) for porous media, as defined by Nellis (Nellis & Kline, 2009). The mass flux of fluid through the porous bed is G (equal to $\dot{m} / (\varepsilon \pi R^2)$), and r_{char} is defined as the characteristic radius of the filler material (Nellis & Kline, 2009), which is equal to $0.25\varepsilon d_r / (1-\varepsilon)$ for spherical solid filler. Here, d_r is the nominal diameter of a rock, if it is not perfectly spherical.

5.2.5 Modification of lumped capacitance method

The model and equations in section 5.2.1 and 5.2.2 use the lumped capacitance method to determine the heat transfer inside the filler material. This method actually ignores the resistance to heat conduction inside the filler material. This will result in the calculated energy going into, or coming out from, a filler material being higher than that in the actual physical process. It is known (Incropera, 2002) that when the Biot number of the heat transfer of a particle is larger than 0.1, the lumped capacitance assumption will result in increased inaccuracy. In order to correct the lumped capacitance approximation for a spherical 'particle' in fluid, Bradshaw et al. (Bradshaw et al., 1970) and Jeffreson (Jeffreson, 1972) proposed to correct the convective heat transfer coefficient between the solid spherical 'particle' and the fluid. The modified heat transfer coefficient is then used in the equations for the transient temperature in the 'particle' from the standard lumped capacitance method. The modified heat transfer coefficient for a spherical 'particle' is:

$$h_p = h\frac{1}{1+Bi/5} \tag{20}$$

The smaller the Bi number [$= h(d_r/2)/k_s$] the smaller the correction that is needed. The modified heat transfer coefficient h_p will be used in Eqs. (10), where h should be replaced by h_p when calculating τ_r.

Figure 6 shows a comparison of the results of dimensionless energy (normalized by the ideal maximum energy change of the 'particle') going in or out from a single spherical 'particle' to a fluid during a transient heat transfer. The energy is quantified based on the local change of internal energy in the particle, and the ideal energy is the internal energy change assuming its temperature completely changed from an initially uniform temperature to the fluid temperature around the particle. The Bi of the case shown in Figure 6 is 2.54, which is close

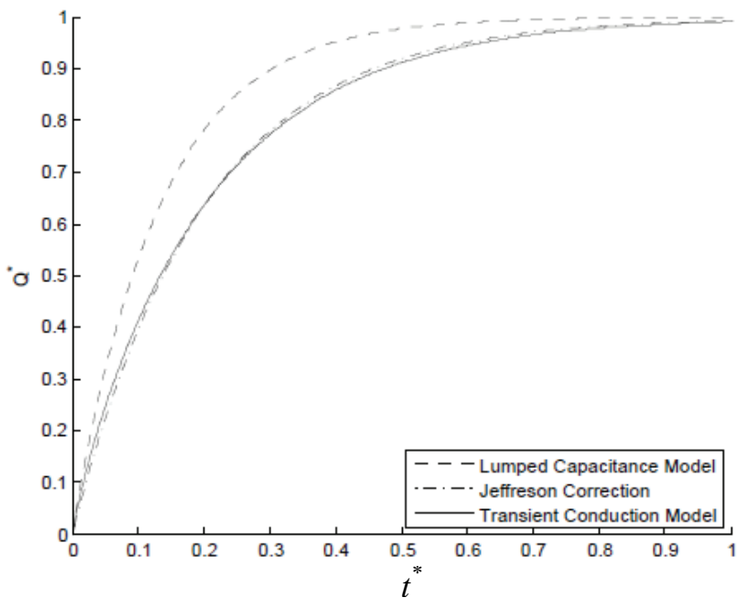

Fig. 6. Jeffreson correction to lumped capacitance heat conduction in a sphere (here only in this figure the dimensionless time is specifically defined as $t^* = t/[(d_r/2)^2/\alpha_s]$)

to the value seen for rocks in typical thermal storage systems. Results from an exact transient heat conduction solution from reference (Incropera, 2002) are compared to the results using the lumped capacitance method, as well as the results obtained using the corrected lumped capacitance method by introducing the modified heat transfer coefficient given in Eq. (20). The heat transfer coefficient used for the comparison was listed in Table 5. Results presented in Fig. 6 indicate that the lumped capacitance method has appreciable discrepancy compared to the exact analytical solution. Results from the Jeffreson correction model agree with the exact transient heat conduction solution very well. Therefore, the Jeffreson correction introducing the modified heat transfer coefficient in the heat transfer model for thermal storage medium and heat transfer fluid is recommended. The Jeffreson correction allows for the thermocline model to remain in a one-dimensional system yet increases the accuracy of the results by accounting for the internal thermal gradient in the packed bed filler material.

Parameters	Value	Unit
d_r	0.04	m
h	355.1	$W/(m^2 \cdot K)$
k_s	2.8	$W/(m \cdot K)$
ρ_s	2630	kg/m^3
C_s	775	$J/(kg \cdot K)$
$\alpha_s = k_s/(\rho_s C_s)$	$1.374 \cdot 10^{-6}$	m^2/s

Table 5. Properties of the solid particle and heat transfer coefficient for the results in Fig. 6

5.2.6 Application of the model to the storage system as shown in Fig. 2(b)

The same governing equations in sections 5.2.1 and 5.2.2 are also applicable to the case shown in Fig. 2(b). However, the porosity in the tank, the heat transfer coefficient h and the heat transfer surface area per unit length, S_s, for the thermal storage tank shown in Fig. 2(b) will be quite different from that in Fig. 2(a). A cross-section of the storage system in Fig. 2(b), including the thermal storage filler material (either solid or liquid) and tubes for the heat transfer fluid, are illustrated in Fig. 7.

An equivalent porosity in the tank is obtained as:

$$\varepsilon = N\frac{d_i^2}{D^2} \tag{21}$$

where N is the number of heat transfer fluid tubes in the storage tank; d_i and D are indicated in Fig. 7.

The heat transfer surface area per unit length in the tank is obtained as:

$$S_s = N\pi d_i \tag{22}$$

The convective heat transfer coefficients inside tubes for either turbulent or laminar fluid flow can be easily obtained from heat transfer textbooks elsewhere. The Reynolds number and Nusselt number for the heat transfer coefficient in tubes are obtained assuming a uniform distribution of total fluid to all the heat transfer fluid tubes.

It is assumed that each heat transfer fluid tube exchanges heat with the storage material in an equivalent control area of diameter D_{eq} as shown in Fig. 7.

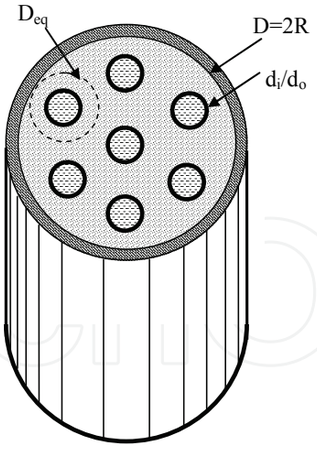

Fig. 7. Schematic of HTF tube and its surrounding thermal storage material (D_{eq} is an equivalent diameter based on the cross sectional area of the container divided by the number of HTF tubes)

The concept of the Jeffreson correction for the lumped capacitance method using a modified heat transfer coefficient is still applicable to the heat conduction in the thermal storage material. However, since the material is not in the form of spherical particles but rather is an integrated solid or liquid, the modified heat transfer coefficient will be different and must be found through analysis.

The following analysis takes one HTF tube and its surrounding thermal storage material for analysis, as shown in Fig. 8. In order to accurately determine the heat going into or out of the filler material in a transient heat conduction process, a transient heat conduction problem is analyzed. This will allow for a comparison of results respectively based on an exact analytical solution, the lumped capacitance method, and the lumped capacitance method with the adoption of a modified heat transfer coefficient.

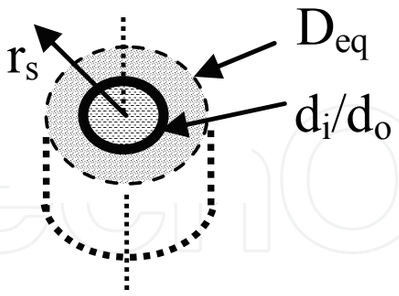

Fig. 8. Physical model of transient heat conduction in a thermally protected "washer"

The analytical solution is for a transient heat conduction problem in a "washer" as shown in Fig. 8. The 'washer' has its outer surface and the two flat surfaces thermally insulated, leaving only the inner surface at $r_s = d_i / 2$ having a convective heat transfer flux.

The mathematical description of this one dimensional problem is

$$\frac{\partial T}{\partial t} = \alpha_s \frac{1}{r_s} \frac{\partial}{\partial r_s} (r_s \frac{\partial T}{\partial r_s}) \tag{23}$$

which is subjected to boundary conditions of:

$$t = 0 \quad T = T_L \tag{24. a}$$

$$t > 0 \text{ at } r_s = d_i / 2 ; \; k_s \frac{\partial T}{\partial r_s} = h(T - T_f) \tag{24. b}$$

$$t > 0 \text{ at } r_s = D_{eq} / 2 ; \; \frac{\partial T}{\partial r_s} = 0 \tag{24. c}$$

Solutions for the energy going into the tube based on the standard lumped capacitance method and solutions of the exact analytical model can be easily obtained. Using results from the exact analytical solution, a modified heat transfer coefficient h_p is introduced to correct the lumped capacitance method for the 'washer'.

$$h_p = h\left(\frac{1}{1 + Bi_{washer} / w_c}\right) \tag{25}$$

where Bi_{washer} is a specially defined Biot number [$= h(d_i / 2) / k_s$] for the "washer"; w_c is a coefficient which depends on the ratio of the washer diameters, D_{eq} / d_i. For a value of $D_{eq} / d_i = 6$ we found w_c = 0.83442 through analysis. Using data for typical thermal storage materials as shown in Table 6, a comparison of results for the dimensionless heat stored in the washer based respectively on the lumped capacitance method, the exact analytical solution, and the modified lumped capacitance method, is shown in Fig. 9. The agreement between the modified lumped capacitance method and the exact analytical solution is very good.

Parameter	Value	Unit
d_i	0.05	m
D_{eq}	0.3	m
h (laminar in tube)	6.88	$W / (m^2 \cdot K)$
k_s	0.57	$W / (m \cdot K)$
ρ_s	1730	kg / m^3
C_s	1.47	$kJ / (kg \cdot K)$
$\alpha_s = k_s / (\rho_s C_s)$	$2.24 \cdot 10^{-7}$	m^2 / s

Table 6. Heat transfer coefficient of HTF-Therminol® VP-1 and properties of primary thermal storage material (molten salt: $Na_2S_2O_3 \cdot 5H_2O$) for the results in Fig. 9

In the energy storage model discussed in sections 5.2.1 and 5.2.2, axial heat conduction in the filler material (solid spherical particles in magnitude of 1.0-10 cm in diameter) is neglected. For integrated solid or liquid thermal storage materials, it is necessary to investigate whether axial heat conduction will be significant. When axial heat conduction in the thermal storage material is considered, the energy balance equation for the thermal storage material is:

$$hS_s(T_s - T_f)dz - (1-\varepsilon)\pi R^2 k_s \frac{\partial^2 T_s}{\partial z^2} dz = -\rho_s C_s (1-\varepsilon)\pi R^2 dz \frac{\partial T_s}{\partial t} \tag{26}$$

Its dimensionless form is:

$$\frac{\partial \theta_s}{\partial t^*} = -\frac{H_{CR}}{\tau_r}(\theta_s - \theta_f) + \frac{k_s}{\rho_s C_s H U}\frac{\partial^2 \theta_s}{\partial z^{*2}} \tag{27}$$

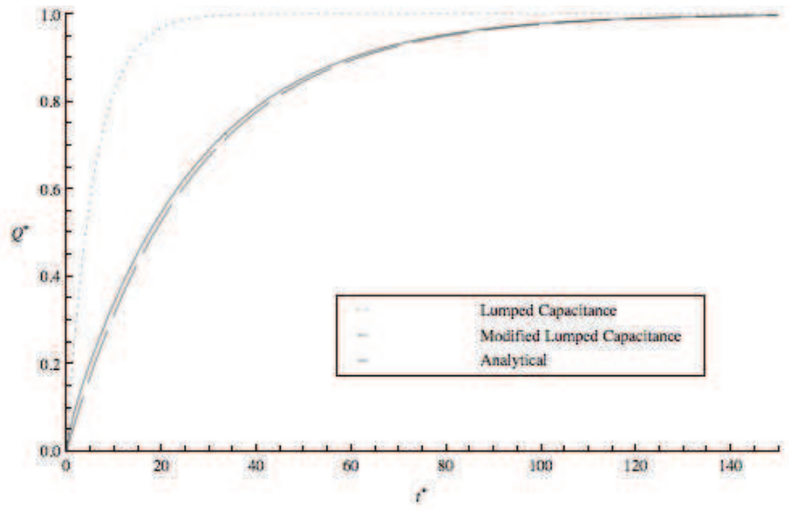

Fig. 9. Comparison of dimensionless energy storage in the 'washer', normalized by the ideal maximum energy change in the 'washer', due to different methods of solution ($Bi_{washer} = h(d_i / 2) / k_s$ =3.0; $D_{eq} / d_i = 6.0$; $t^* = t / [(d_i / 2)^2 / \alpha_s]$; w_c = 0.83442)

The parameter cluster of $k_s / (\rho_s C_s HU)$ is a dimensionless term. If it is sufficiently large, the axial conduction term in Eq. (27) may not be dropped off. A basic effect of significant axial heat conduction is that it will destroy the thermocline effect—a temperature gradient with hot material being on top of cold. This can lower the thermal storage performance in general. Therefore, to take into account the axial heat conduction effect, a similar correction via the introduction of another factor to the modified heat transfer coefficient is proposed. This results in a new modified heat transfer coefficient of:

$$h_p = h\left(\frac{1}{1 + Bi_{washer} / w_c}\right)\left(\frac{1}{1 + \dfrac{k_s}{\rho_s C_s H U}}\right) \tag{28}$$

For most thermal storage materials, such as rocks, molten salts, concrete, soil, and sands, the value of $k_s / (\rho_s C_s HU)$ is very small (in the order of 1×10^{-6}); while other terms in Eq.(27) are in the order of 1.0. Therefore, the axial heat conduction effect in the thermal storage material in Eq. (27) is negligible.

5.2.7 Application of the model to the storage system with PCM

For thermal storage with phase-change involved, the PCM can be enclosed in capsules to form a packed bed as shown in Fig. 2(a), or simply put in a storage tank that has heat transfer tubes inside as shown in Fig. 2(b). The governing equations discussed above are still

applicable to the heat transfer at locations where either phase change has not yet occurred or has already been completed. However, at locations undergoing phase change, the energy equations must account for the melting or solidification process (Halawa & Saman, 2011; Wu et al., 2011). The key feature in a melting or solidification process is that the temperature of the material stays constant.
Considering the energy balance for the thermal storage material:

$$hS_s(T_m - T_f) = -\Gamma\rho_s(1-\varepsilon)\pi R^2 \frac{d\Phi}{dt} \tag{29}$$

where Γ is the fusion energy of the material, and Φ is the ratio of the liquid mass to the total mass in the control volume of dz. For melting, Φ increases from 0 to 1.0, while for solidification it decreases from 1.0 to 0.
Considering the invariant of the temperature of the material during a phase change process, the energy balance equation for HTF is:

$$\frac{hS_s}{\rho_f C_f \varepsilon \pi R^2}(T_m - T_f) = \frac{\partial T_f}{\partial t} + U\frac{\partial T_f}{\partial z} \tag{30}$$

Equation (29) and (30) can be reduced to dimensionless equations by introducing the same group of dimensionless parameters:

$$\frac{1}{\tau_r}(\theta_m - \theta_f) = \frac{\partial \theta_f}{\partial t^*} + \frac{\partial \theta_f}{\partial z^*} \tag{31}$$

$$-\frac{H_{CR}}{\tau_r}\psi(\theta_m - \theta_f) = \frac{d\Phi}{dt^*} \tag{32}$$

where a new dimensionless parameter $\psi = (T_H - T_L)C_s / \Gamma$ is introduced. Since the phase change temperature is known, Eqs. (31) and (32) can be solved separately.

5.3 Numerical methods and solution to governing equations

5.3.1 Solution for the case of no phase change

A number of analyses and solutions to the heat transfer governing equations of a working fluid flowing through a packed-bed have been presented in the past (Schumann, 1929; Shitzer & Levy, 1983; McMahan, 2006; Beasley, 1984; Zarty & Juddaimi, 1987). As the pioneering work, Schumann (Schumann, 1929) presented a set of equations governing the energy conservation of fluid flow through porous media. Schumann's equations have been widely adopted in the analysis of thermocline heat storage utilizing solid filler material inside a tank. His analysis and solutions were for the special case where there is a fixed fluid temperature at the inlet to the storage system. In most solar thermal storage applications this may not be the actual situation. To overcome this limitation, Shitzer and Levy (Shitzer & Levy, 1983) employed Duhamel's theorem on the basis of Schumann's solution to consider a transient inlet fluid temperature to the storage system. The analysis of Schumann, and Shitzer and Levy, however, still carry with them some limitations. Their method does not consider a non-uniform initial temperature distribution. For a heat storage system, particularly in a solar thermal power plant, heat charge and discharge are cycled daily. The initial temperature field of a heat charge process is dictated by the most recently completed

heat discharge process, and vice versa. Therefore, non-uniform and nonlinear temperature distribution is typical for both charge and discharge processes. To consider a non-uniform initial temperature distribution and varying fluid temperature at the inlet in a heat storage system, numerical methods have been deployed by researchers in the past.

To avoid the long mathematical analysis necessary in analytical solutions, numerical methods used to solve the Schumann equations were discussed in the literature by McMahan (McMahan, 2006, 2007), and Pacheco et al. (Pacheco et al., 2002), and demonstrated in the TRNSYS software developed by Kolb and Hassani (Kolb & Hassani, 2006). Based on the regular finite-difference method, McMahan provided both explicit and implicit discretized equations for the Schumann equations. Whereas the explicit solution method had serious stability issues, the implicit solution method encountered an additional computational overhead, thus requiring a dramatic amount of computation time. The solution for the complete power plant with thermocline storage provided by the TRNSYS model in Kolb's work (Kolb & Hassani, 2006) cites the short time step requirement for the differential equations of the thermocline as one major source of computer time consumption. To overcome the problems encountered in the explicit and implicit methods, McMahan et al. also proposed an infinite-NTU method (McMahan, 2006, 2007). This model however is limited to the case in which the heat transfer of the fluid compared to the heat storage in fluid is extremely large.

The present study has approached the governing equations using a different numerical method (Van Lew et al., 2011). The governing equations have been reduced to dimensionless forms which allow for a universal application of the solution. The dimensionless hyperbolic type equations are solved numerically by the method of characteristics. This numerical method overcomes the numerical difficulties encountered in McMahan's work—explicit, implicit, and the restriction on infinite-NTU method (McMahan, 2006, 2007). The current model yields a direct solution to the discretized equations (with no iterative computation needed) and completely eliminates any computational overhead. A grid-independent solution is obtained at a small number of nodes. The method of characteristics and the present numerical solution has proven to be a fast, efficient, and accurate algorithm for the Schumann equations.

The non-dimensional energy balance equations for the heat transfer fluid and filler material can be solved numerically along the characteristics (Courant & Hilbert, 1962; Polyanin, 2002; Ferziger, 1998). Equation (9) can be reduced along the characteristic $t^* = z^*$ so that:

$$\frac{D\theta_f}{Dt^*} = \frac{1}{\tau_r}(\theta_r - \theta_f) \tag{33}$$

Separating and integrating along the characteristic, the equation becomes:

$$\int d\theta_f = \int \frac{1}{\tau_r}(\theta_r - \theta_f)dt^* \tag{34}$$

Similarly, Eq.(12) for the energy balance for the filler material is reposed along the characteristic z^* =constant so that:

$$\frac{d\theta_r}{dt^*} = -\frac{H_{CR}}{\tau_r}(\theta_r - \theta_f) \tag{35}$$

The solution for Eq. (35) is very similar to that for Eq. (33) but with the additional factor of H_{CR}. The term H_{CR} is simply a fractional ratio of fluid heat capacitance to filler heat capacitance. Therefore, the equation for the solution of θ_r will react with a dampened speed when compared to θ_f, as the filler material must have the capacity to store the energy being delivered to it, or vice versa. Finally, separating and integrating along the characteristic for Eq.(35) results in:

$$\int d\theta_r = \int -\frac{H_{CR}}{\tau_r}(\theta_r - \theta_f)dt^* \tag{36}$$

There are now two characteristic equations bound to intersections of time and space. A discretized grid of points, laid over the time-space dimensions will have nodes at these intersecting points. A diagram of these points in a matrix is shown in Fig. 10. In space, there are i = 1, 2, . . . ,M nodes broken up into step sizes of Δz^* to span all of z^*. Similarly, in time, there are j = 1, 2, . . . ,N nodes broken up into time-steps of Δt^* to span all of t^*. Looking at a grid of the ϑ nodes, a clear picture of the solution can arise. To demonstrate a calculation of the solution we can look at a specific point in time, along z^* where there are two points, $\vartheta_{1,1}$ and $\vartheta_{2,1}$. These two points are the starting points of their respective characteristic waves described by Eq. (33) and (36). After the time Δt^* there is a third point $\vartheta_{2,2}$ which has been reached by both wave equations. Therefore, Eq. (34) can be integrated numerically as:

$$\int_{\vartheta_{1,1}}^{\vartheta_{2,2}} d\theta_f = \int_{\vartheta_{1,1}}^{\vartheta_{2,2}} \frac{1}{\tau_r}(\theta_r - \theta_f)dt^* \tag{37}$$

The numerical integration of the right hand side is performed via the trapezoidal rule and the solution is:

$$\theta_{f_{2,2}} - \theta_{f_{1,1}} = \frac{1}{\tau_r}\left(\frac{\theta_{r_{2,2}} + \theta_{r_{1,1}}}{2} - \frac{\theta_{f_{2,2}} + \theta_{f_{1,1}}}{2}\right)\Delta t^* \tag{38}$$

where $\theta_{f_{1,1}}$ is the value of θ_f at $\vartheta_{1,1}$, and $\theta_{f_{2,2}}$ is the value of θ_f at $\vartheta_{2,2}$, and similarly so for θ_r.
The integration for Eq. (36) along z^* =constant is:

$$\int_{\vartheta_{2,1}}^{\vartheta_{2,2}} d\theta_r = \int_{\vartheta_{2,1}}^{\vartheta_{2,2}} [-\frac{H_{CR}}{\tau_r}(\theta_r - \theta_f)]dt^* \tag{39}$$

The numerical integration of the right hand side is also performed via the trapezoidal rule and the solution is:

$$\theta_{r_{2,2}} - \theta_{r_{2,1}} = -\frac{H_{CR}}{\tau_r}\left(\frac{\theta_{r_{2,2}} + \theta_{r_{2,1}}}{2} - \frac{\theta_{f_{2,2}} + \theta_{f_{2,1}}}{2}\right)\Delta t^* \tag{40}$$

Equations (38) and (40) can be reposed as a system of algebraic equations for two unknowns, $\theta_{f_{2,2}}$ and $\theta_{r_{2,2}}$, while θ_f and θ_r at grid points $\vartheta_{1,1}$ and $\vartheta_{2,1}$ are known.

$$\begin{bmatrix} 1+\dfrac{\Delta t^*}{2\tau_r} & -\dfrac{\Delta t^*}{2\tau_r} \\ -\dfrac{H_{CR}\Delta t^*}{2\tau_r} & 1+\dfrac{H_{CR}\Delta t^*}{2\tau_r} \end{bmatrix} \begin{bmatrix} \theta_{f_{2,2}} \\ \\ \theta_{r_{2,2}} \end{bmatrix} = \begin{bmatrix} \theta_{f_{1,1}}\left(1-\dfrac{\Delta t^*}{2\tau_r}\right)+\theta_{r_{1,1}}\dfrac{\Delta t^*}{2\tau_r} \\ \theta_{f_{2,1}}\left(\dfrac{H_{CR}\Delta t^*}{2\tau_r}\right)+\theta_{r_{2,1}}\left(1-\dfrac{H_{CR}\Delta t^*}{2\tau_r}\right) \end{bmatrix} \tag{41}$$

Cramer's rule (Ferziger, 1998) can be applied to obtain the solution efficiently. It is important to note that all coefficients/terms in Eq.(41) are independent of z^*, t^*, θ_f, and θ_r, thus they can be evaluated once for all. Therefore, the numerical computation takes a minimum of computing time, and is much more efficient than the method applied in references (McMahan, 2006, 2007).

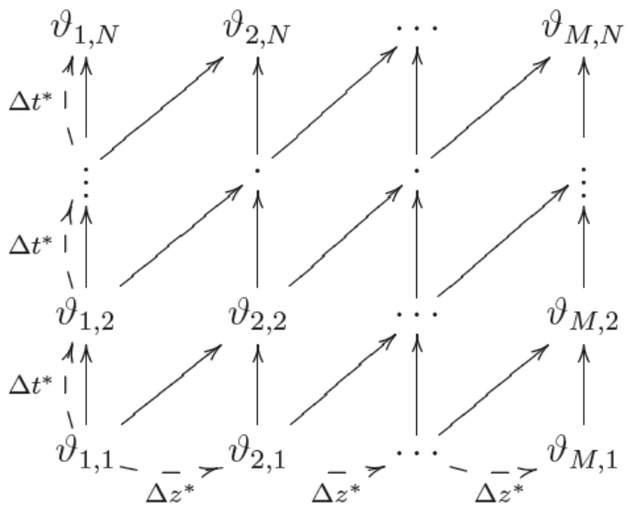

Fig. 10. Diagram of the solution matrix arising from the method of characteristics

From the grid matrix in Fig.10 it is seen that the temperatures of the filler and fluid at grids $\vartheta_{i,1}$ are the initial conditions. The temperatures of the fluid and filler at grid $\vartheta_{1,1}$ are the inlet conditions which vary with time. The inlet temperature for the fluid versus time is given. The filler temperature (as a function of time) at the inlet can be easily obtained using Eq.(12), for which the inlet fluid temperature is known. Now, as the conditions at $\vartheta_{1,1}$, $\vartheta_{1,2}$, and $\vartheta_{2,1}$ are known, the temperatures of the rocks and fluid at $\vartheta_{2,2}$ will be easily calculated from Eq.(41).

Extending the above sample calculation to all points in the ϑ grid of time and space will give the entire matrix of solutions in time and space for both the rocks and fluid. While the march of Δz^* steps is limited to $z^* = 1$ the march of time Δt^* has no limitation.

The above numerical integrations used the trapezoidal rule; the error of such an implementation is not straightforwardly analyzed but the formal accuracy is on the order of $O(\Delta t^{*2})$ for functions (Ferziger, 1998) such as those solved in this study.

5.3.2 Solutions for the case with phase change

For the governing equations of the phase change case, the adopted convention of having the z-direction coordinate always follow the flow direction is preserved, such that for heat

charging, z=0 is for the top of a tank, and for heat discharging, z=0 is for the bottom of a tank. The two governing equations (Eq. (31) and Eq.(32)) for the phase change process can be discretized using finite control volume methodology:

$$\frac{1}{\tau_r}(\theta_m - \theta_{f(i)}^{t^*+\Delta t^*}) = \frac{\theta_{f(i)}^{t^*+\Delta t^*} - \theta_{f(i)}^{t^*}}{\Delta t^*} + \frac{\theta_{f(i)}^{t^*+\Delta t^*} - \theta_{f(i-1)}^{t^*+\Delta t^*}}{\Delta z^*} \tag{42}$$

$$-\frac{H_{CR}}{\tau_r}\psi(\theta_m - \theta_{f(i)}^{t^*+\Delta t^*}) = \frac{\Phi_i^{t^*+\Delta t^*} - \Phi_i^{t^*}}{\Delta t^*} \tag{43}$$

From Eq.(42) the fluid temperature $\theta_{f(i)}^{t^*+\Delta t^*}$ can be solved, which is then used in Eq. (43) to solve for the fusion ratio $\Phi_i^{t^*+\Delta t^*}$.

The procedures for finding the solution of phase change problem are as follows:

1. Solve the non-phase-change governing equation analytically using Eq.(12) for the phase change material for the inlet point.
2. Monitor the temperature at each time step as given by Eq.(12), and see if the temperature at a time step is greater than the fusion temperature, if yes, the solution for that and subsequent time steps are to be solved using the phase change equation (Eq. (43)
3. For each time step solved using Eq (43), monitor the fusion ratio, Φ ; when it becomes larger than 1.0 then the solution for that and subsequent time steps are to be solved using the non-phase-change governing equation (Eq.(12)) for the remainder of the required time.
4. March a spatial step forward and repeat all of the above steps. However, now in part (1) of this procedure, Eq.(41) must be used to solve the temperatures of both the fluid and PCM for time steps before phase change starts; and also in part (3) of this procedure Eq.(41) should be used to solve the temperatures of the fluid and PCM for steps after the phase change is over. The repetition of parts (1) to (3) of this procedure is to be continued until all the spatial steps are covered.

6. Results from simulations and experimental tests

6.1 Numerical results for the temperature variation in a packed bed

The first analysis of the storage system was done on a single tank configuration of a chosen geometry, using a filler and fluid with given thermodynamic properties. The advantage of having the governing equations reduced to their dimensionless form is that by finding the values of two dimensionless parameters (τ_r and H_{CR}) all the necessary information about the problem is known. The properties of the fluid and filler rocks, as well as the tank dimensions, which determined τ_r and H_{CR} for the example problem, are summarized in Table 7.

The numerical computation started from a discharge process assuming initial conditions of an ideally charged tank with the fluid and rocks both having the same high temperature throughout the entire tank, i.e. $\theta_f = \theta_s = 1$. After the heat discharge, the temperature distribution in the tank is taken as the initial condition of the following charge process. The discharge and charge time were each set to 4 hours. The fluid mass flow rate was determined such that an empty (no filler) tank was sure to be filled by the fluid in 4 hours.

With the current configuration, after five discharge and charge cycles the results of all subsequent discharge processes were identical—likewise for the charge processes. It is therefore assumed that the solution is then independent of the first-initial condition. The data presented in the following portions of this section are the results from the cyclic discharge and charge processes after 5 cycles.

ε	τ_r	H_{CR}	H	R	**t**
0.25	0.0152	0.3051	14.6	m	7.3 m
Fluid (Therminol® VP-1) properties:					
T_H=395 °C;		T_L=310 °C;	ρ_f =753.75 kg/m^3;	C_f=2474.5 J/(kg K);	
k_f=0.086W/(m K);		$\dot{m}$ =128.74 kg/s;		μ_f =1.8×10^{-4} $Pa\cdot s$;	
Filler material (granite rocks) properties:					
ρ_s = 2630 kg/m3;		C_s=775 J/(kg K);	k_s=2.8 W/(m K);	d_r= 0.04 m;	

Table 7. Dimensions and parameters of a thermocline tank (Van Lew et al., 2011)

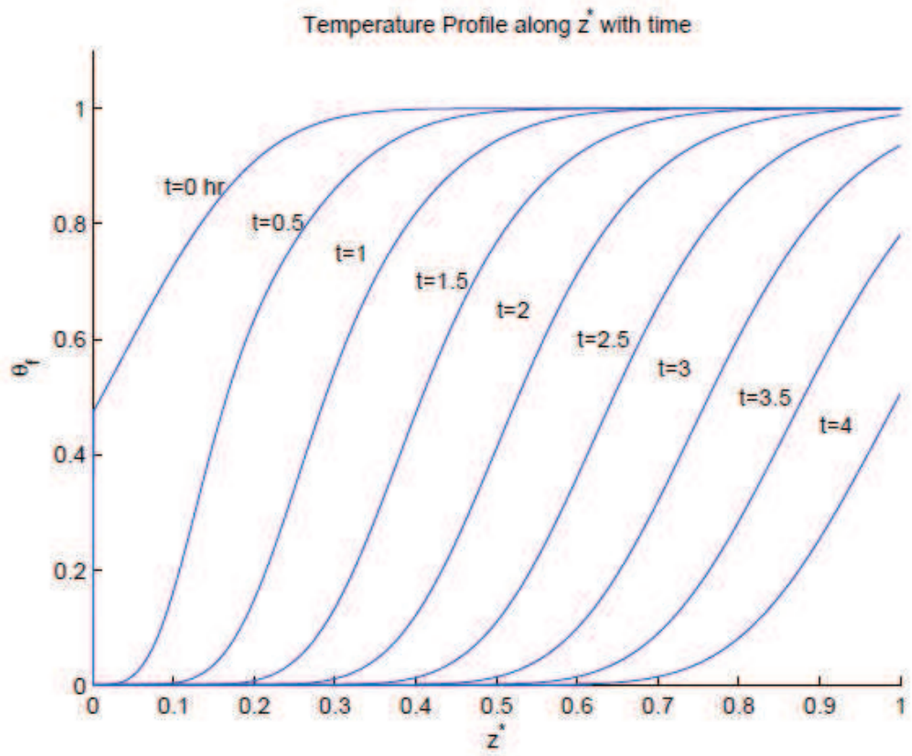

Fig. 11. Dimensionless fluid temperature profile in the tank for every 0.5 hours

Shown in Fig. 11 are the temperature profiles in the tank during a discharge process, in which cold fluid enters into the tank from bottom of the tank. The location of $z^* = 0$ is at the bottom of a tank for a discharge process. The temperature profile evolves as discharging proceeds, showing the heat wave propagation and the high temperature fluid moving out of

the storage tank. The fluid temperature at the exit ($z^* = 1$) of the tank gradually decreases after 3 hours of discharge. At the end of the discharge process, the temperature distribution along the tank is shown in Fig. 12. At this time the fluid and rock temperatures, θ_f and θ_s respectively (θ_s is denoted by θ_r when the filler material is rock), in the region with z^* below 0.7 are almost zero, which means that the heat in the rocks in this region has been completely extracted by the passing fluid. In the region from $z^* = 0.7$ to $z^* = 1.0$ the temperature of the fluid and rock gradually becomes higher, which indicates that some heat has remained in the tank.

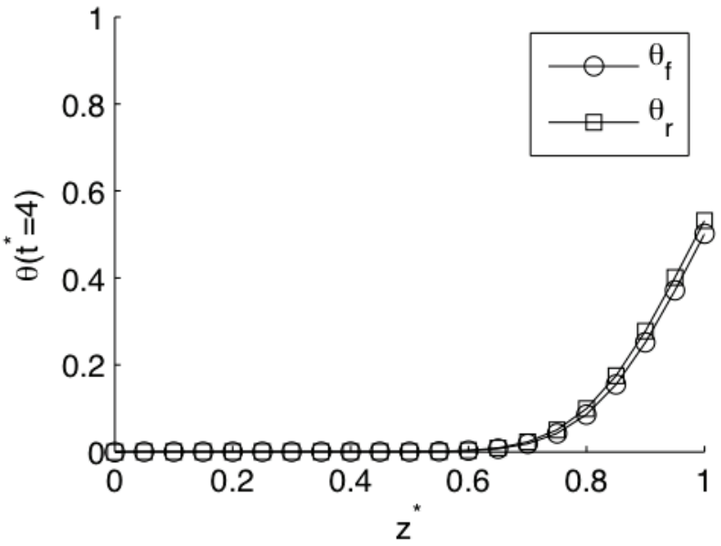

Fig. 12. Dimensionless temperature distribution in the tank after time t^* = 4 of discharge (Here θ_r is used to denote θ_s , as rocks are used as the storage material in the example).

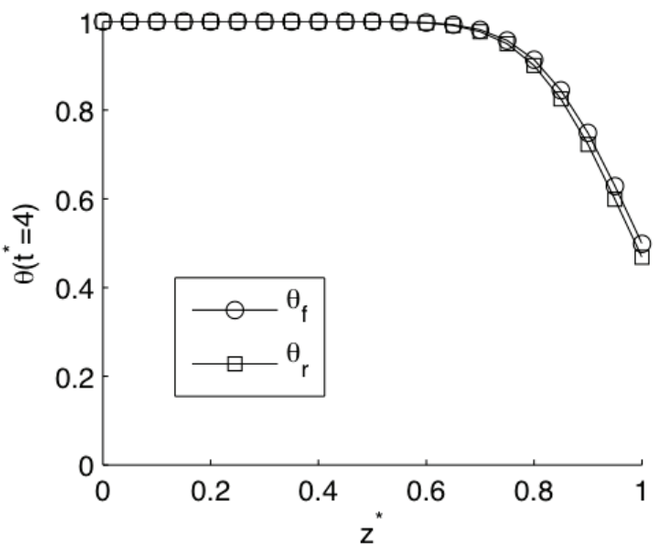

Fig. 13. Dimensionless temperature distribution in the tank after time t^* = 4 of charge

(Here θ_r is used to denote θ_s, as rocks are used as the storage material in the example)
A heat charge process exhibits a similar heat wave propagation scenario. The temperature for the filler and fluid along the flow direction is shown in Fig. 13 after a 4 hour charging process. During a charge process, fluid flows into the tank from the top, where z^* is set as zero. It is seen that for the bottom region (z^* from 0.7 to 1.0) the temperatures of the fluid and rocks decrease significantly. A slight temperature difference between heat transfer fluid and rocks also exists in this region.

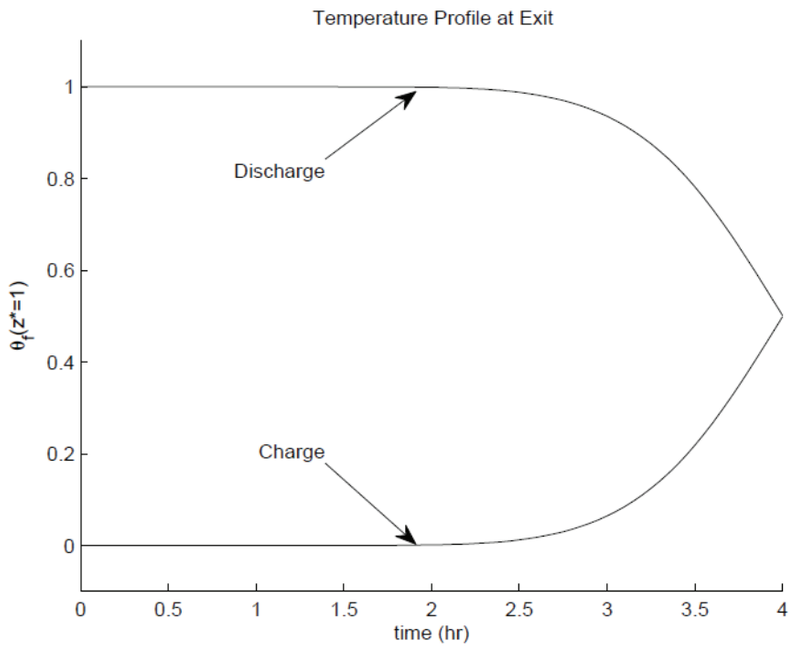

Fig. 14. Dimensionless temperature histories of the exit fluid at z^* = 1 for charge and discharge processes

The next plots of interest are the variation of θ_f at $z^* = 1$ as dimensionless time progresses for a charging or discharging process. Figure 14 shows the behavior of θ_f at the outlet during both charge and discharge cycles. For the charge cycle, θ_f begins to increase when all of the initially cold fluid has been ejected from the thermocline tank. For the present thermocline tank, the fluid that first entered the tank at the start of the cycle has moved completely through the tank at $t^* = 1$, which also indicates that the initially-existing cold fluid of the tank has been ejected from the tank. Similarly, during the discharge cycle, after the initially-existing hot fluid in the tank has been ejected, the cold fluid that first entered the tank from the bottom at the start of the cycle has moved completely through the tank at $t^* = 1$. At $t^* = 2.5$, or t=2.5 hours, the fluid temperature θ_f starts to drop. This is because the energy from the rock bed has been significantly depleted and incoming cold fluid no longer can be heated to θ_f = 1 by the time it exits the storage tank.
The above numerical results agree with the expected scenario as described in section 4. To validate the above numerical method, analytical solutions were obtained using a Laplace Transform method by the current authors (Karaki, et al, 2010), which were only possible for cases with a constant inlet fluid temperature and a simple initial temperature profile. Results compared in Fig. 15 are obtained under the same operational conditions—starting from a

fully charged initial state and run for 5 iterations of cyclic discharge and charge processes. The fluid temperature distribution along the tank (z^*=0 for bottom of the tank) from numerical results agrees with the analytical results very well. This comparison essentially proves the effectiveness and reliability of the numerical method developed in the present study.

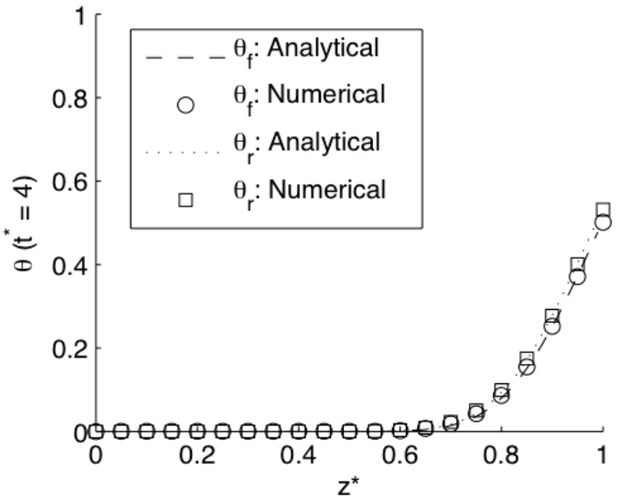

Fig. 15. Comparison of numerical and analytical results of the temperature distribution in the tank after time t^* = 4 of a discharge (Here θ_r is used to denote θ_s , as rocks are used as the storage material in the example)

Based on the results shown in Fig. 15, the temperature distribution along z^* at the end of a charge is nonlinear. This distribution will be the initial condition for the next discharge cycle. Similarly a discharge process will result in a nonlinear temperature distribution, which will be the initial condition for the next charge. It is evident that the analytical solutions developed by Schumann (Schumann, 1929) could not handle this type of situation.

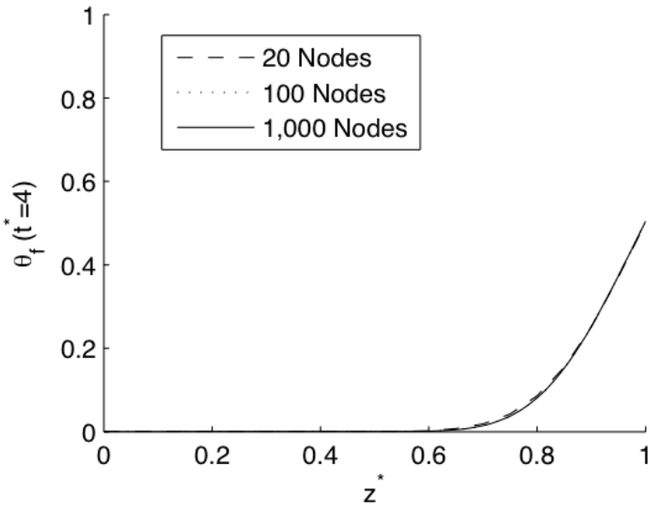

Fig. 16. Comparison of dimensionless temperature distributions in the tank after time t^* = 4 of discharge for different numbers of discretized nodes

Another special comparison was made to demonstrate the efficiency of the method of characteristics at solving the dimensionless form of the governing equations. Shown in Fig. 16 are the temperature profiles at $t^* = 4$ obtained by using different numbers of nodes (20, 100, and 1000) for z^*. The high level of accuracy of the current numerical method, even with only 20 nodes, demonstrates the accuracy and stability of the method with minimal computing time.

6.2 Comparison of modeling results with experimental data from literature

6.2.1 Temperature variations in charge processes

The authors have conducted experimental tests (Karaki at al., 2011). The test conditions for a given heat charge process are listed in Table 8, which also shows the dimensionless parameters. As shown in Fig. 17, at the initial time the thermocline tank has a uniform temperature equal to room temperature. The temperature readings from the thermocouples at the top of the tank provide the inlet fluid temperatures in a charge process.

Tank Length	0.65(m)			Initial temperature			21.9 (°C)
Tank inner diameter	0.241 (m)			High temperature			79.82 (°C)
Rock nominal diameter	0.01 (m)			Low temperature			21.9 (°C)
Oil flow rate	1.0 (Liter/min.)			Porosity			0.324
Density of rocks	2632.8 kg/m^3			$\Pi_c = t_c / (H / U)$			7.2511
Charging period t_c	70.08 (min.)			τ_r			0.1262
Rock heat capacity	790 (J/(kg K))			H_{CR}			0.4068
Time (s)	0	856	1713	2570	3427	4284	
Dimensionless time t^*	0	1.45	2.9	4.35	5.80	7.25	

Table 8. Conditions of a heat charging test (HTF is Xceltherm 600 by Radco Industries)

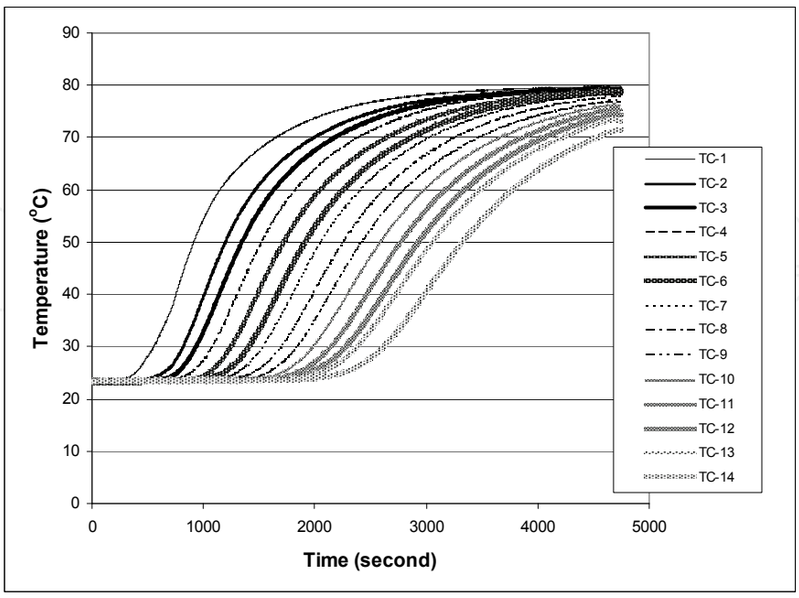

Fig. 17. Temperatures in the center of the tank along the height of 65 cm for a charging process (Thermocouples were set every 5cm)

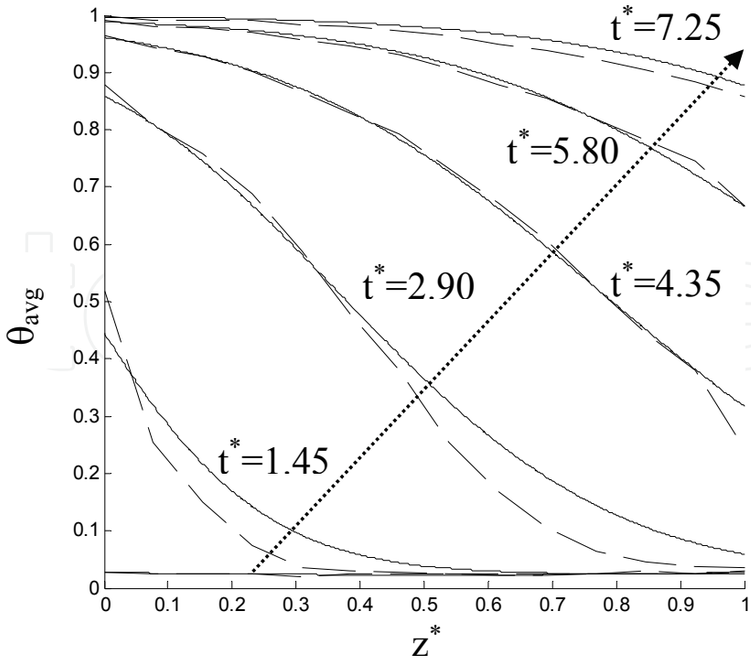

Fig. 18. The temperature distribution along the height in the tank at different time points (Solid lines are from simulation results and dashed lines are from experimental tests)

Based on the temperature measurements, the temperature in the tank increases gradually and at the end of the charging process, the temperatures at all the locations are sufficiently high. The temperature distribution along the height in the tank at different times is shown in Fig. 18. Obviously at the end of the charge, the temperature at the top of the tank (at z*=0) is high. Using the initial temperature distribution and the inlet fluid temperature, together with the properties listed in Table 8, numerical simulation results were obtained and are shown in Fig. 18 for the average temperature of the fluid and rocks. The real time and the dimensionless time are listed in Table 8. The agreement between the experimental data and the modeling simulation is very satisfactory.

The thermal storage performance test results of a thermocline tank reported in the literature (Pacheco et al., 2002) was also referenced to validate the current modeling work. The experimental tests used eutectic molten salt ($NaNO_3$-KNO_3, 50% by 50%) as the heat transfer fluid and quartzite rocks and silica sands as the filler material. Thermocouples in the test apparatus were imbedded in the packed-bed. Temperatures in the tank at different height locations were recorded during a two-hour heat discharge process after the tank was charged for the same length of time. The storage tank dimensions, packed-bed porosity, and properties of the fluid and filler material are listed in Table 9.

Using the modeling of section 5, the heat charge followed by heat discharge was simulated. In Fig. 19, the predicted temperatures at several height locations of the tank at different time instances during the discharge process were compared to the experimental data reported (Pacheco et al., 2002). The trend of temperature curves from the modeling prediction and the experiment is quite consistent. Considering the uncertainties in the experimental test and the properties of materials considered, the agreement between the experimental data and the modeling prediction is quite satisfactory. This comparasion firmly validates the current modeling and its numerical solution method.

ε	τ_r	H_{CR}	H	R	**t**
0.22	0.0041	0.2733	6.1m	1.5m	2 hr
Molten salt $NaNO_3$-KNO_3 properties:					
T_H=396 °C;	T_L=290 °C;	ρ_f =1733 kg/m³;	C_f=1550 J/(kg K);		
k_f=0.57 W/(m K);	$\dot{m}$ =7.0 kg/s;	μ_f = 0.0021 $Pa \cdot s$;			
Quartzite rocks/sands mixture properties:					
ρ_s = 2640 kg/m3;	C_s=1050 J/(kg K);	k_s=2.5 W/(m K);	d_r= 0.015 m;		

Table 9. Dimensions and parameters of a thermocline tank for the test in literature (Pacheco et al., 2002)

Tank Length measured	0.65(m)			Initial temperature			129.0 (°C)
Tank inner diameter	0.241 (m)			High temperature			129.0 (°C)
Rock nominal diameter	0.01 (m)			Low temperature			56.0 (°C)
Oil flow rate	1.96 (Liter/min.)			Porosity			0.324
Density of rocks	2632.8 kg/m³			$\Pi_d = t_d / (H / U)$			8.0596
Charging period t_c	39.74 (min)			τ_r			0.1044
Rock heat capacity	790 (J/(kg K))			H_{CR}			0.4210
Time (s)	0	476.2	952.5	1428.7	1905.0	2381.2	
Dimensionless time t^*	0	1.61192	3.22384	4.83576	6.44768	8.0596	

Table 10. Conditions of a discharge test

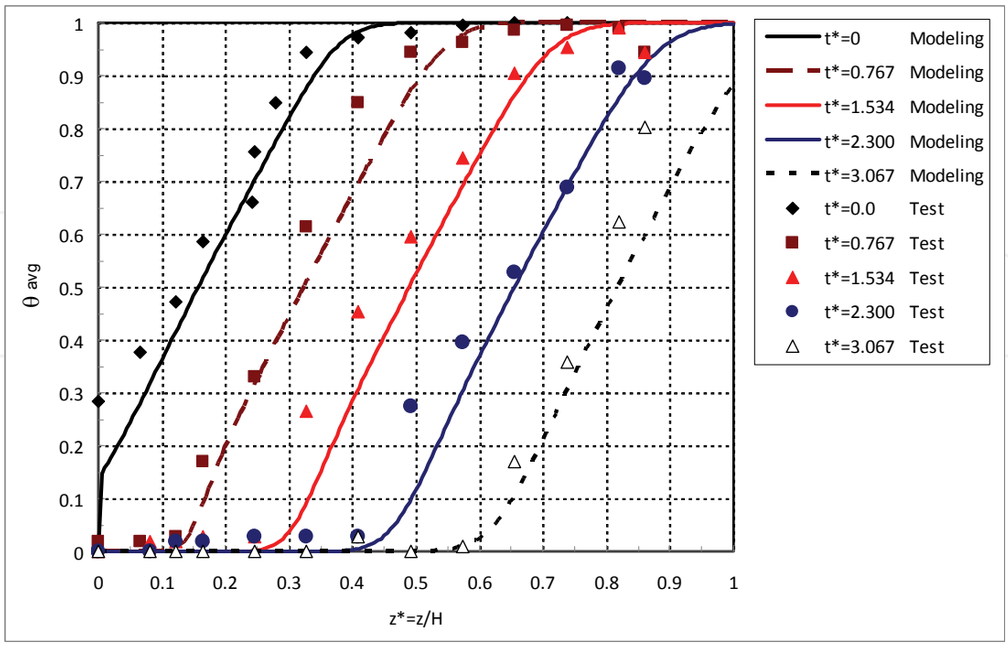

Fig. 19. Comparison of modeling predicted results with experimental data from reference (Pacheco et al., 2002)

6.2.2 Temperature variations in a discharge process

A heat discharge experiment was conducted under the conditions listed in Table 10, which also includes the dimensionless parameters. Shown in Fig. 20 is the temperature variation versus time at different locations in the tank along the tank height. The thermocouples at the top (z^*=1.0) of the tank measure the temperature of the discharged fluid. The degradation of discharged fluid temperature is clearly shown in the figure.

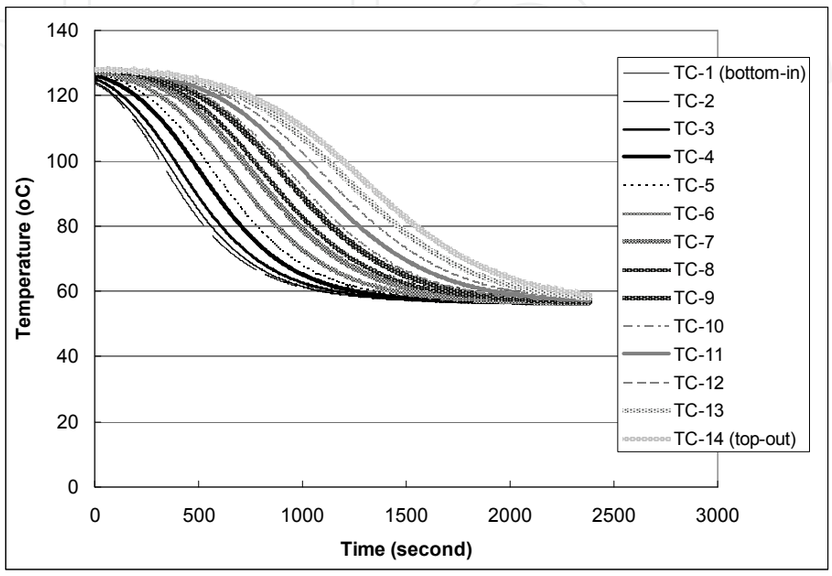

Fig. 20. Temperatures in the center of the tank along the height of 65 cm for a discharging process (Thermocouples were set every 5cm)

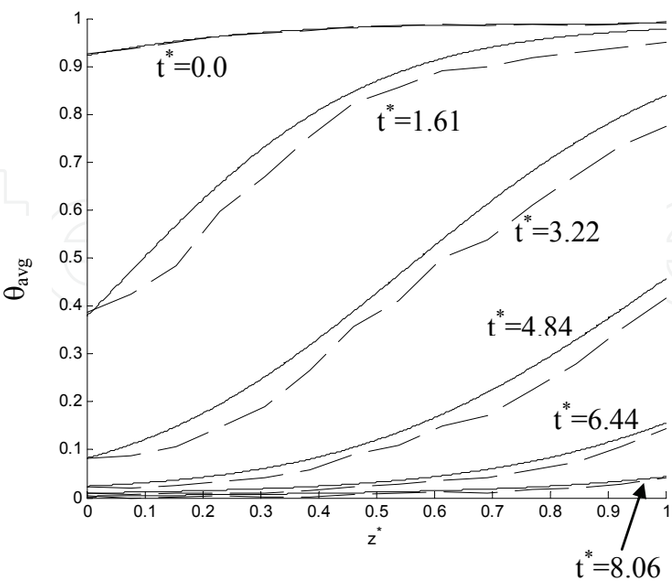

Fig. 21. The temperature distribution along the height in the tank at different time points (Solid lines are from simulation results and dashed lines are from experimental tests)

The temperature distribution along the height in the tank at different times is shown in Fig. 21. At the end of the discharge, the temperature on top of the tank (at z*=1) becomes low, which means that stored energy has been discharged. Using the measured initial temperature distribution and the inlet fluid temperature (at z*=1) together with the properties listed in Table 10, numerical simulation results were obtained and are compared with the test results in Fig. 21. The real time and the dimensionless time are listed in Table 10. Again, the agreement between the experimental data and the modeling simulation is satisfactory.

6.3 Correlation of energy delivery effectiveness to dimensionless parameters

Based on the above discussion and the dimensionless governing equations obtained in section 5.2.3, the energy delivery effectiveness, η, is a function of four dimensionless parameters, Π_c / Π_d, Π_d, τ_r, and H_{CR}. Solutions of the dimensionless governing equations for energy charge and discharge allow us to develop a database so that a series of charts and diagrams for $\eta = f(\Pi_c / \Pi_d, \Pi_d, \tau_r, H_{CR})$ may be prepared for reference by engineers in the design of thermocline storage tanks. Illustrated in Fig. 22 is a configuration of a group of database charts for a given Π_d, in which multiple graphs, each with a specific τ_r, may be provided. In each graph, multiple curves, each with a given H_{CR}, for the energy storage effectiveness η versus Π_c / Π_d are provided. To build a large database, more graphs in the same configuration can be provided covering a large range of Π_d values.

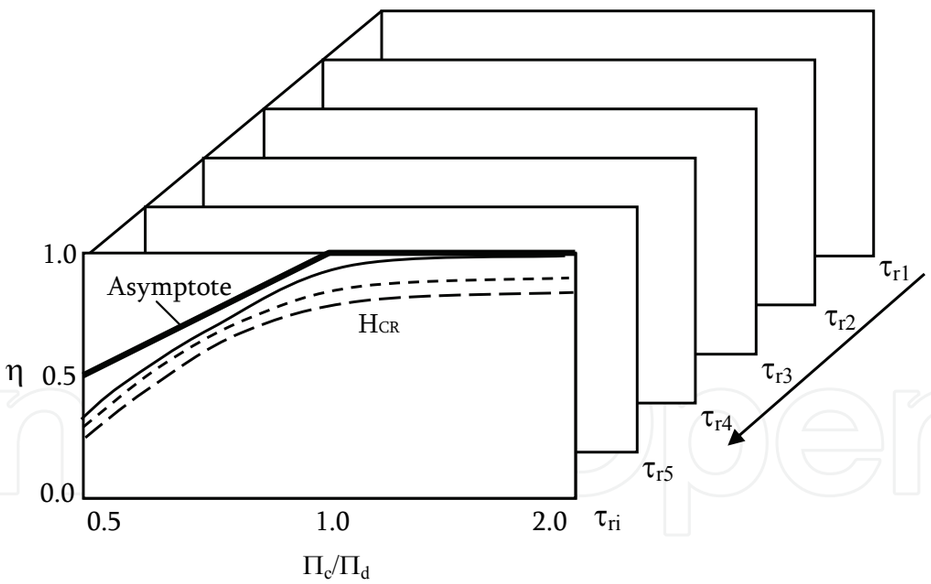

Fig. 22. Configuration of a group of database charts including multiple graphs of η versus Π_c / Π_d at a fixed Π_d

It is easy to understand that under the same mass flow rate and a desired Π_d, the energy delivery effectiveness will increase with the increase of Π_c / Π_d. The asymptote of the energy delivery effectiveness is due to an ideal thermal storage system, in which η can be exactly 1.0 if the energy charge period is equal to or larger than that of the discharge ($\Pi_c / \Pi_d \geq 1.0$). For any non-ideal thermocline system η can only approach 1.0.

Figure 23 shows four charts of η versus Π_c / Π_d at Π_d =4.0. Each chart is for a specific τ_r with multiple curves for different H_{CR}. All the data of energy delivery effectiveness were obtained based on several cyclic operations of the energy charge and discharge, and the results are consequently independent of the number of cycles. More charts with wide range of Π_d, τ_r, and H_{CR} may be developed. However, in actual design practice, the ranges of Π_d, τ_r, and H_{CR} are not very wide and specific charts can be easily prepared.

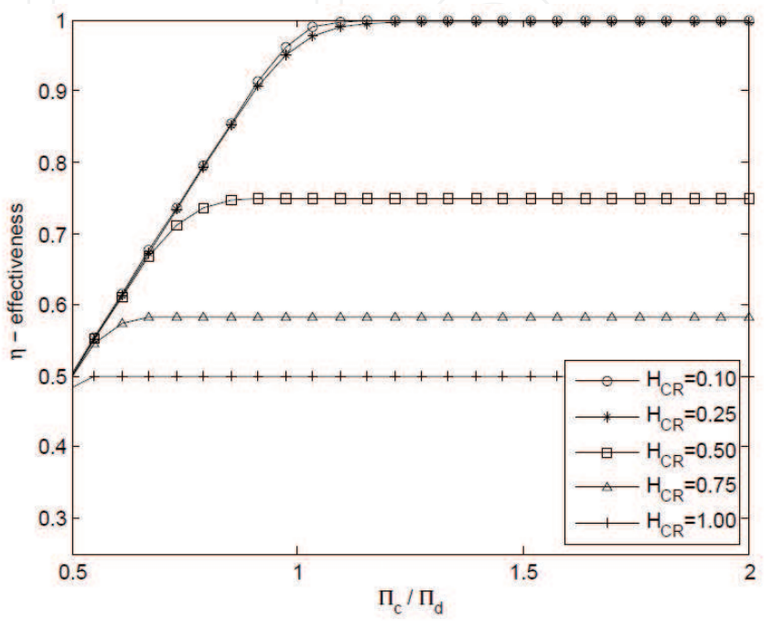

(a) $\tau_r = 0.01$

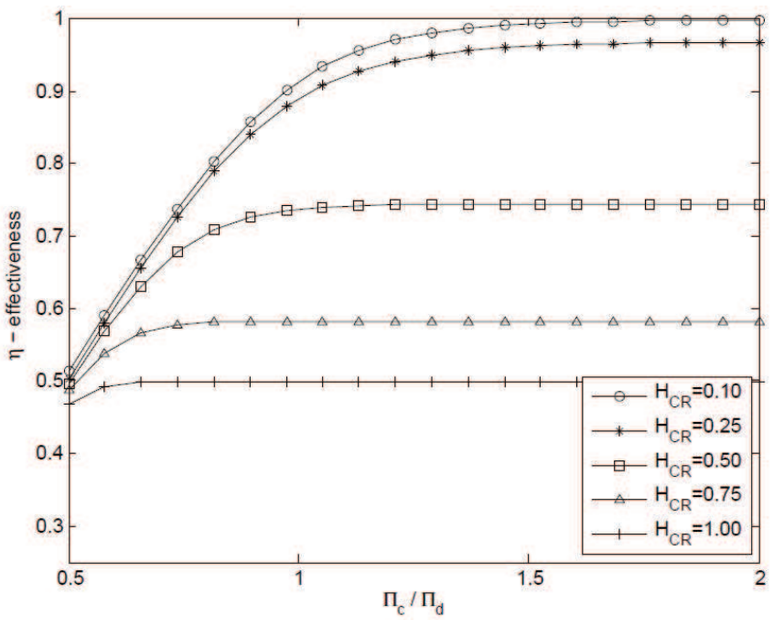

(b) $\tau_r = 0.04$

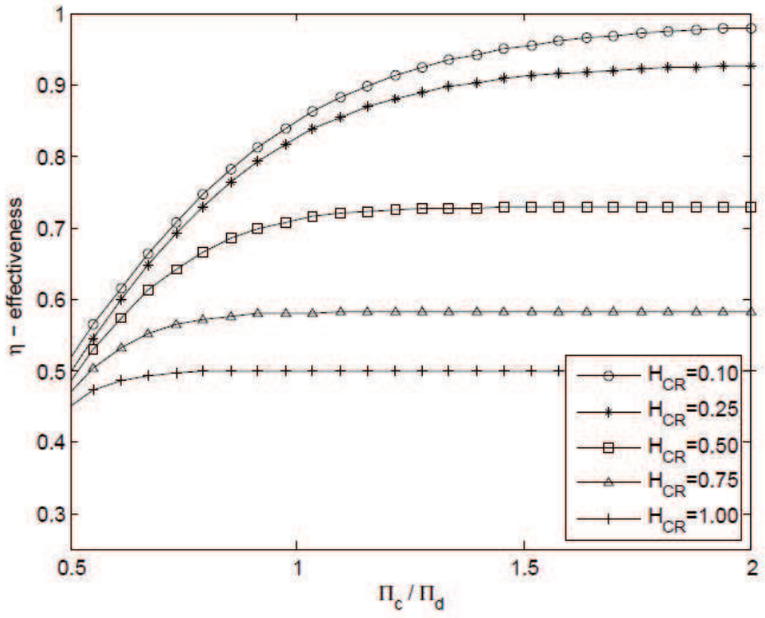

(c) $\tau_r = 0.1$

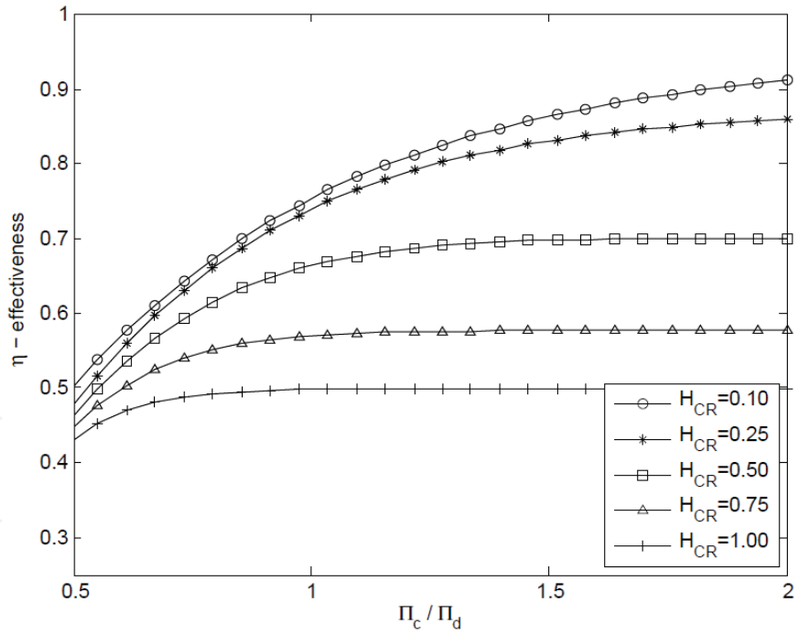

(d) $\tau_r = 0.2$

Fig. 23. Multiple graphs from modeling results for energy storage effectiveness versus Π_c / Π_d at Π_d =4.0

Observing the above four graphs one can easily draw the following conclusions:

1. The energy delivery effectiveness never reaches 1.0 if $\Pi_c / \Pi_d < 1.0$. This proves that only for an ideal thermocline storage tank can $\eta = 1.0$ at $\Pi_c / \Pi_d = 1.0$.

2. With the decrease of τ_r, η will increase. For example, at a ratio of $\Pi_c / \Pi_d = 1.5$ and $H_{CR} = 0.25$, the energy delivery effectiveness approaches 1.0 when τ_r changes from 0.2 to 0.01. This is because a decrease of τ_r is due to an increase in the volume of the storage tank.
3. It is understood that a small H_{CR} corresponds to the case where $(\rho C)_s$ is relatively large when compared to $(\rho C)_f$, and therefore the energy storage capability is improved, and η can approach 1.0 easier. On the other hand, when the void fraction in a packed bed approaches 1.0, it will make $H_{CR} \to \infty$, and the thermal storage effectiveness can approach that of an ideal case. However, in most practical applications, a low void fraction in a thermocline tank is required for the purpose of using less heat transfer fluid, and therefore a smaller H_{CR} value is practical and preferable.
4. For cases where η could never approach 1.0, even at large Π_c / Π_d values, it is obviously attributable to the fact that the storage tank is too small, and reselection of a larger storage tank is needed.

Designers for a thermal storage system often need to calibrate or confirm that a given storage tank can satisfy an energy delivery requirement. Under such a circumstance, the dimensions of the storage tank and the power plant operational conditions are known, which means the values of τ_r, Π_d, and H_{CR} are essentially given. One can easily check whether over a range of values of Π_c / Π_d the energy delivery effectiveness η can approach 1.0.

7. Procedures of sizing and design of a thermal storage system

The required operational conditions of the power plant dictate the size of the thermocline storage tank. The relevant operational conditions include: electrical power, thermal efficiency of the power plant, the extended period of operation based on stored thermal energy, the required high temperature of the heat transfer fluid from the storage tank, and the low temperature of the fluid returned from the power plant, the specific choice of heat transfer fluid and thermal storage material, as well as the packing porosity in a thermocline tank. The design analysis using the general charts provided in the present study will include the following steps:

1. Select a minimum required volume for a thermocline tank using Eqs. (1) and (3).
2. Choose a radius, R, and the corresponding height, H, from the minimum volume decided in step (1). Using these dimensions, the parameters— Π_d, τ_r, H_{CR} for a thermocline tank with filler material, can be evaluated, where Π_d is determined based on the required operational time.
3. Look up the design charts (such as those in Fig. 23) and see if an energy delivery effectiveness of 1.0 can be achieved. Often the energy delivery effectiveness will not approach 1.0 for the first trial design. This is because the first trial uses a minimum volume. However, with the results from the first trial one can predict the required height or volume of the tank necessary to decrease τ_r and Π_d in the same proportion. A couple of trail iterations may be needed to eventually satisfy the criterion of η closing to 1.0.

If the energy delivery effectiveness from step (1) cannot approach 1.0 even if a large Π_c / Π_d is chosen, one actually has two ways to improve the effectiveness during the second trial. These are to decrease H_{CR}, or decrease both τ_r and Π_d in the same proportion. However, H_{CR} is determined by properties of the fluid and filler material, which has very limited

options, and therefore a decrease of τ_r and Π_d is more practical. The decrease of τ_r can be done by an increase of the height of a storage tank. This means that to achieve an effectiveness of 1.0 one has to increase the size of the storage tank. When the height of tank is increased, Π_d decreases accordingly since it depends on the height of the tank.

Occasionally, a calibration analysis requires a designer to find a proper time period of energy charge that can satisfy the needed operation time of a power plant. The known parameters will be the tank volume, τ_r, as well as H_{CR} at a required operation period of Π_d. The first step of the calibration should be the examination of the criterion given in Eq. (3), from which a minimum tank volume can be chosen. If the minimum tank volume is satisfied, the second step of calibration will be to find a proper Π_c / Π_d that can make the energy delivery effectiveness approach 1.0. Graphs including curves at the required H_{CR} and the given τ_r and Π_d must be looked up. Conclusions can be easily made depending on whether the energy delivery effectiveness can approach 1.0 for a particular value of Π_c / Π_d.

Two practical examples of thermocline thermal storage tank design are provided to help industrial designers practice the design procedures proposed in this work. Readers can easily repeat the design procedures while using their specific material parameters and operational conditions.

7.1 Design example 1—a system as shown in Fig. 2(a)

A solar thermal power plant has 1.0 MW electrical power output at a thermal efficiency of 20%. The heat transfer fluid used in the solar field is Therminol® VP-1. The power plant requires high and low fluid temperatures of 390 °C and 310 °C, respectively. River rocks are used as the filler material and the void fraction of packed rocks in the tank is 0.33. The required time period of energy discharge is 4 hours, the storage tank diameter is chosen to be 8 m. The rock diameter is 4 cm.

The solution is discussed as follows:

1. Making use of Eqs. (1) to (3) and the above given details on the power plant, as well as the properties of Therminol® VP-1, we can find a necessary mass flow rate of 25.34 kg/m^3 and an ideal tank height of 9.59 m. The minimum volume of the storage tank can be determined from Eq. (3). Here, the ideal volume is used in the first trial of the design. Using Eqs. (19) and (20) we find the modified heat transfer coefficient to be 32.05 W/(m^2 K). With this information, the values of H_{CR}, Π_d, and τ_r are found to be 0.451, 3.03, and 0.0227, respectively. Given in Fig. 24 is a chart for Π_d =3 and τ_r =0.0227 at various values of H_{CR} and Π_c / Π_d. It is seen that on the curve of H_{CR} =0.45, there is no time ratio Π_c / Π_d that allows the energy delivery effectiveness to be close to 1.0. Therefore, the ideal volume chosen will not satisfy the energy storage need.
2. One option to provide the ability to store and deliver more energy and approach an effectiveness of 1.0 is to increase the height of the storage tank. When the height is increased to 12 m, the values of Π_d and τ_r changed to 2.42 and 0.0181, respectively. Figure 25 gives the chart for Π_d =2.42 and τ_r =0.0181. It is seen on the curve of H_{CR} = 0.45 that at the time period ratio, Π_c / Π_d =1.2, the energy delivery effectiveness approaches 0.99. This should be an acceptable design.

In this example, compared to an ideal thermal storage tank, the rock-packed-bed thermocline tank uses about 40.0% of the heat transfer fluid. To avoid the temperature degradation of the heat transfer fluid in a required discharge time period, a 20% longer charging time than discharging time is always applied in every charge and discharge cycle.

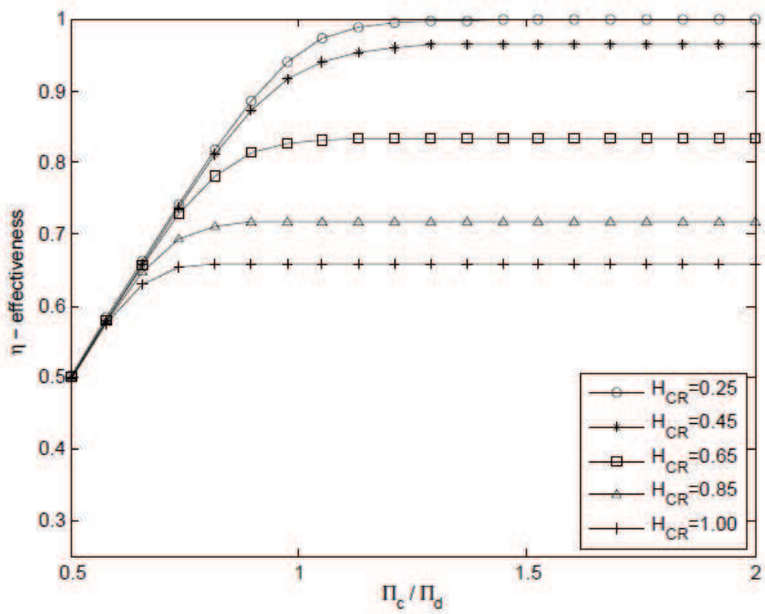

Fig. 24. Energy delivery effectiveness versus Π_c / Π_d at Π_d =3 and τ_r =0.0227

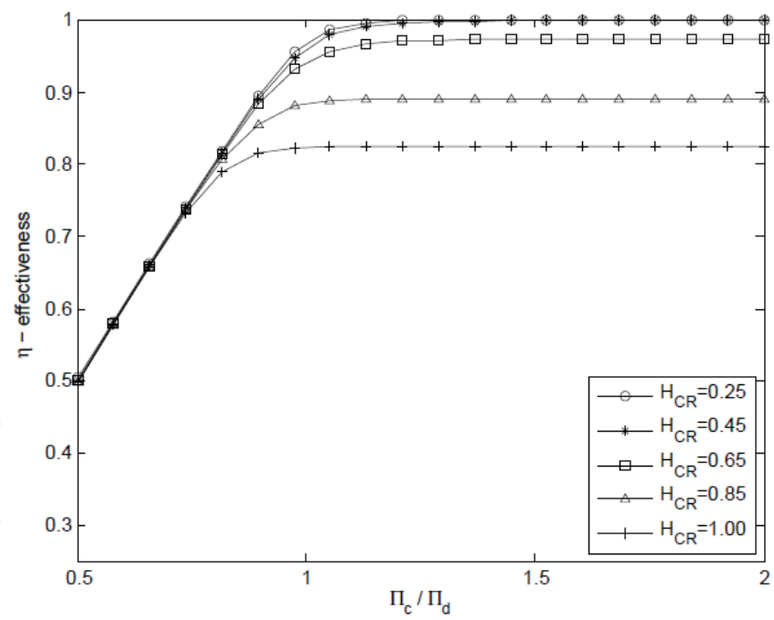

Fig. 25. Energy delivery effectiveness versus Π_c / Π_d at Π_d =2.42 and τ_r =0.0181

7.2 Design example 2—a system as shown in Fig. 2(b)

For the same solar thermal power plant and operational conditions as in Example 1, the thermal storage primary material is molten salt with properties of $\rho = 1680 kg / m^3$, $C_s = 1560 J / (kg \cdot K)$, and $k_s = 0.61 W / (m \cdot K)$. The heat transfer fluid, Hitec (Bradshaw & Siegel, 2009), flows in multiple heat transfer tubes, in the same arrangement as shown in Fig.

2(b). The required time period of energy discharge is 4 hours, the storage tank diameter is 8 m. The study will find the storage tank height.
The solution and design procedures are as follows:

3. Following the same procedure as seen in Example 1, we determine the mass flow rate to be 40.35 kg/m^3, and the ideal tank diameter and height to be 8 m and 6.44 m respectively. It is assumed that we have 8448 steel pipes (with inner diameters of 0.025m) in the storage tank, and that the heat transfer fluid flows in all of the pipes with an equal flow rate. The void fraction ε is found to be 0.33, and the heat transfer surface area per unit of length of the tank is found to be S_s =1327 m. The modified heat transfer coefficient inside a pipe for laminar flow heat transfer is used based on the correction using Eqs. (23) to (25), where the correction coefficient for the washer is w_c = 3.69894 for the ratio of $D_{eq} / d_i = 1.74$. The minimum volume of the tank is used in the first trial of the design. The dimensionless values of H_{CR}, Π_d, and τ_r are 0.522, 3.032, and 0.221, respectively. Given in Fig. 26 is a chart for Π_d =3.032 and τ_r =0.221 at various values of H_{CR} and Π_c / Π_d. The figure shows that at an H_{CR} value of 0.50 (close to 0.522) it is impossible to get an energy efficiency of 1.0 for attempted time ratios of Π_c / Π_d up to 2.0.

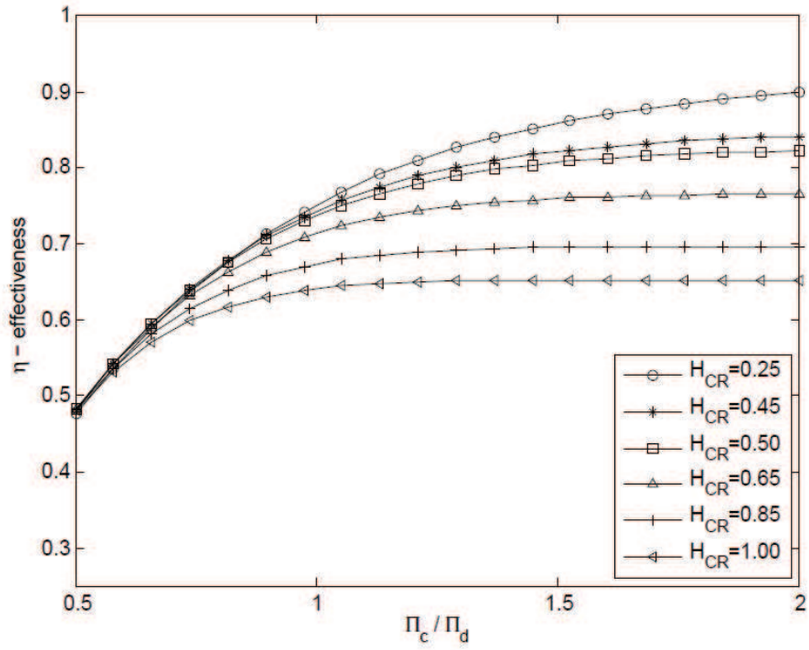

Fig. 26. Energy delivery effectiveness versus Π_c / Π_d at Π_d =3.032 and τ_r =0.221

To increase the energy delivery efficiency, a new tank height of 2.1 times that of the ideal volume tank is used. This makes the value of Π_d and τ_r be 1.444 and 0.105, respectively. Figure 27 shows the curves for Π_d =1.444 and τ_r =0.105. It is seen that at an H_{CR} value of 0.50 (close to 0.522) and a time period ratio, Π_c / Π_d, of 1.2, the energy delivery effectiveness can reach 0.96.
Note that in the finalized storage tank (with a height of 13.5 m), the volume of heat transfer fluid takes 69% of the volume of an ideal thermal storage tank (with a height of 6.44 m). The energy delivery effectiveness reached 0.96 if the charging time period was kept 20% longer than the required discharge time. Obviously, the weak heat transfer between the HTF and

the primary thermal storage material in Example 2 is responsible for the much larger ratio of the actual volume compared to the volume of the ideal storage tank. In Example 1 the ratio of the actual volume of the finalized storage tank is only 1.25 times that of the volume of its corresponding ideal storage tank. Therefore, it is important that in order to improve the energy delivery efficiency, the heat transfer between the fluid and thermal storage material must be improved, for example, by using pipes with fins. Nevertheless, this type of thermal storage system, as in Example 2, still saves 31% of the heat transfer fluid.

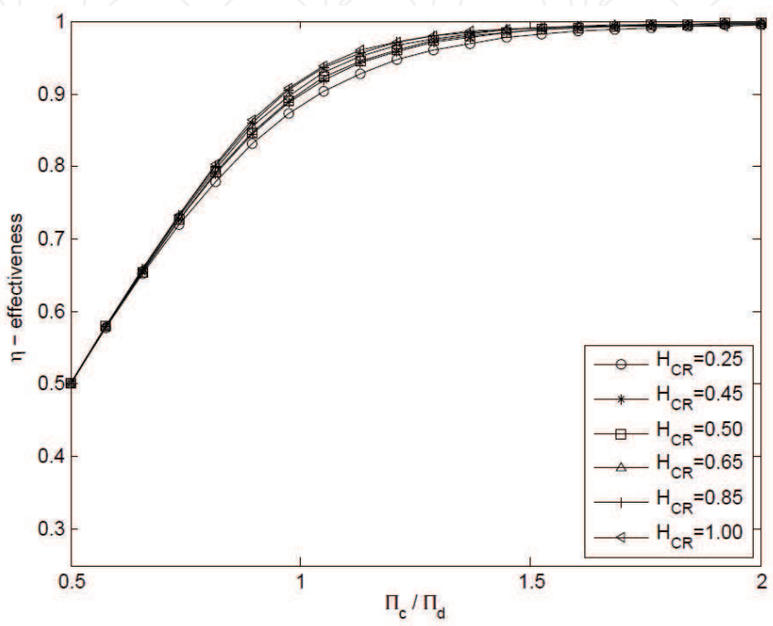

Fig. 27. Energy delivery effectiveness versus Π_c / Π_d at Π_d =1.444 and τ_r =0.105

Thermal energy storage in soil (Nassar et al., 2006), concrete (Zhang et al., 2004; Laing at al., 2006; Reuss et al., 1997), and in sands (Wyman, 1980) has similar features to that of the Example 2. When the heat transfer performance (the multiplication of the heat transfer coefficient and the heat transfer area) between the heat transfer fluid and thermal storage material is poor, the energy delivery effectiveness can be rather low. If the temperature degradation of the discharged fluid is a big concern, for example in a power plant, the thermal storage system in Example 2 may need enhancement of the heat transfer performance between the heat transfer fluid and thermal storage material.

8. Concluding remarks

Thermal energy storage is very important to the development of concentrated solar thermal power technologies. Thermal energy storage is also particularly attractive for large capacity energy storage. It is becoming more and more common for industrial engineers to be required to size and design thermal storage systems. Therefore, it is necessary to provide a general analytical tool for the sizing and design of thermal energy storage systems.

The details of the analytical model provided in this book chapter will help researchers and industrial engineers to understand the behavior of the heat transfer and energy transport between heat transfer fluid and thermal energy storage material. Two examples for the

practical design of the size of thermal storage systems were provided for readers to practice the design process concretely. The authors believe that the currently developed charts, relating the energy storage efficiency to the properties and parameters of a thermal storage system, are of great potential to help industrial engineers performing sizing calculations for thermal storage systems. In this regard, the publication of this chapter is a significant and timely event.

Due to space limitations, this chapter did not provide a large number of the developed charts for thermal storage system sizing and design. However, the authors are currently working to provide a handbook including a large number of design charts covering a wide range of design parameters that industry will need. It is hoped that the handbook will be available to readers in the near future.

9. Acknowledgement

The authors are grateful for the support provided by the US Department of Energy and the National Renewable Energy Laboratory, under DOE Award Number DE-FC36-08GO18155, and the US Solar Thermal Storage LLC. The Support from the Idaho National Laboratory under award number 00095573 for phase change thermal storage is also gratefully acknowledged.

10. Nomenclature

a_f	The cross section area of a storage tank (m^2)
Bi	Biot number ($= L_p h / k_s$)
C	Heat capacity ($J / kg \cdot {}^oC$)
d_r	Nominal diameter of a single filler 'particle' (rocks) (m)
D	Diameter of a storage tank (m)
D_{eq}	Equivalent diameter (m)
$\hbar$	Enthalpy of fluid at a location along the axis (J / kg)
h	Heat transfer coefficient ($W / m^2 {}^oC$)
h_p	Modified heat transfer coefficient ($W / m^2 {}^oC$)
H	Length or height of a storage tank (m)
H_{CR}	A dimensionless parameter
k	Thermal conductivity ($W / m {}^oC$)
Lp	Characteristic length of 'particles' for Biot number.
$\dot{m}$	Mass flow rate (kg/s)
N	Number of tubes for heat transfer fluid in a storage tank
Pr	Prandtl number
$\dot{Q}$	Thermal energy involved per unit of time (W)
Q	Thermal energy involved (J)
r	Average radius of the filler material (rocks) (m)
R	Radius of the storage tank (m)
Re	Modified Reynolds number for porous media
Ss	Surface area of filler material per unit length of the storage tank (m)
t	Time (sec)
T_H	High temperature of fluid from solar field (°C)
T_L	Low temperature of fluid from power plant (°C)

U Fluid velocity in the axial direction in the storage tank (*m/s*)
V Volume (m^3)
z Location of a fluid element along the axis of the tank (*m*)

Greek symbols

α_s Thermal diffusivity (= $k_s / (\rho_s C_s)$) [m²/s]
ε Porosity of packed bed in a storage tank.
η_s Thermal storage efficiency.
η_T Thermal efficiency of a solar power plant.
Γ Fusion energy of thermal storage material (J / kg)
μ Dynamic viscosity ($Pa \cdot s$)
Π Dimensionless charge or discharge time
τ_r A dimensionless parameter
ρ Density (kg / m^3)
θ Dimensionless temperature.

Subscript

c Energy charge process
d Energy discharge process
f Thermal fluid
ref A required reference value
r Rocks
s Filler material (rocks), the primary thermal storage material.
z Location along the axis of the tank

Superscript

* Dimensionless values

11. References

Abdoly, M.A., Rapp, D., 1982, Theoretical and experimental studies of stratified thermocline storage of hot water, Energy Conversion and Management, Vol. 22, No. 3, 1982, pp. 275-285.

Beasley, D.E., and Clark, J.A., 1984, Transient response of a packed bed for thermal energy storage, International Journal of Heat and Mass Transfer, 27(9), pp. 1659 –1669.

Becker, M., 1980, Comparison of heat transfer fluid for use in solar thermal power stations. Electric Power Systems Research, 3 (1980) 139-150.

Bradshaw R.W., Siegel N.P., 2009, Development of molten nitrate salt mixtures for concentrating solar power systems, paper no. 11538, proc. SolarPACES, Berlin, Germany, 2009.

Bradshaw, A.V., Johnson, A., McLachlan, N.H., Chiu, Y-T., 1970, Heat transfer between air and nitrogen and packed beds of non-reacting solids, Trans. Instn Chem. Engrs, Vol. 48, 1970, pp. T77-T84.

Brosseau, D., Kelton, J.W., Ray, D., Edgar, M., Chisman, K., and Emms, B., 2005, Testing of thermocline filler materials and molten-salt heat transfer fluids for thermal energy storage systems in parabolic trough power plants, Journal of Solar Energy Engineering, 127(1), pp. 109–116.

Canada, S., Brosseau, D. A., and Price, H., 2006, Design and Construction of the APS 1MWe parabolic trough power plant, ASME Conference Proceedings, 2006(47454), pp. 91–98.

Conway, J.H. & Sloane, N.J.H., 1998, Sphere Packings, Lattices and Groups, (Third Edition). ISBN 0-387-98585-9.

Courant, R., Hilbert, D., 1962, *Methods of Mathematical Physics, Volume II*, Wiley-Interscience.

Ferziger, J.H., 1998, *Numerical Methods for Engineering Applications*. Wiley-Interscience.

Gil, A., Medrano, M., Martorell, I., Lazaro, A., Dolado, P., Zalba, B., and Cabeza, L.F., 2010, State of the art on high temperature thermal energy storage for power generation, part 1—concepts, materials and modellization, Renewable and Sustainable Energy Reviews, 14(1): 31-55.

Halawa, E., Saman, W., 2011, Thermal performance analysis of a phase change thermal storage unit for space heating, Renewable Energy 36 (2011) 259-264.

Hales, T.C., 2006, Historical overview of the Kepler conjecture, Discrete & Computational Geometry. an International Journal of Mathematics and Computer Science 36 (1): 5–20.

Hasnain S.M., 1998, Review on sustainable thermal energy storage technologies, part I: heat storage materials and techniques. Energy Convers. Mgmt. 1998, Vol. 39: 1127–1138.

Herrmann, U., and Kearney, D.W., 2002, Survey of thermal energy storage for parabolic trough power plants, Journal of Solar Energy Engineering, 124(2), pp. 145–152.

Herrmann, U., Kelly, B., and Price, H., 2004, Two-tank molten salt storage for parabolic trough solar power plants, Energy, 29(5-6), pp. 883 – 893.

Incropera, F.P., and DeWitt, D.P., 2002, Introduction to Heat Transfer, fourth ed. John Wiley and Sons, Inc.

Jeffreson, C.P., 1972, Prediction of breakthrough curves in packed beds: 1. applicability of single parameter models, American Institute of Chemical Engineers, 18(2), pp. 409-416.

Karaki, W., Van Lew, J.T., Li, P.W., Chan, C.L., Stephens, J., 2010, Heat transfer in thermocline storage system with filler materials: analytical model, Proceedings of the ASME 2010 4th International Conference on Energy Sustainability, ES2010-90209, May 17-22, 2010, Phoenix, Arizona, USA.

Karaki, W., Li, P.W., Van Lew, J.T., Valmiki, M.M., Chan, C.L., Stephens, J., 2011, Experimental investigation of thermal storage processes in a thermocline storage tank, Submitted to ASME 5th International Conference on Energy Sustainability, ESFuelCell2011, August 7-10, Washington DC, USA

Kays, W. M., Crawford, M. E., and Weigand, B., 2005, Convective Heat and Mass Transfer, fourth ed. McGraw Hill.

Kolb, G.J., 1998, Economic evaluation of solar-only and hybrid power towers using molten-salt technology, Solar Energy, Vol. 62 (1), January 1998, pp. 51-61.

Kolb, G.J., and Hassani, V., 2006, Performance analysis of thermocline energy storage proposed for the 1 mw saguaro solar trough plant, *ASME Conference Proceedings*, 2006 (47454), pp. 1–5.

Krane, R.J., and Krane, M.J.M., 1992, The optimum design of stratified thermal energy storage systems—part II: completion of the analytical model, presentation and interpretation of the results, Journal of Energy Resources Technology, 114(3), pp. 204–208.

Laing, D., Steinmann, W. D., Viebahn, P., Gräter, F., and Bahl, C., 2010, Economic analysis and life cycle assessment of concrete thermal energy storage for parabolic trough power plants, Journal of Solar Energy Engineering, 132, 041013.

Laing, D, Steinmann, W.D., Tamme, R., Richter, C., 2006, Solid media thermal storage for parabolic trough power plants, Solar Energy, Vol. 80, pp. 1283-1289.

Li, P.W., 2008, Energy storage is the core of renewable energy technologies, IEEE Nanotechnology Magzine, December 2008, pp. 3-18.

Li, P.W., Van Lew, J.T., Chan, C.L., Karaki, W., Stephens, J., 2010, Similarity and generalized analysis of efficiencies of thermal energy storage systems, Submitted to Journal of Renewable Energy, 2010.

McMahan, A. C., 2006, Design and optimization of organic Rankine cycle solar-thermal power plants, Master's thesis, University of Wisconsin, Madison, Wisconsin.

McMahan, A.C., Klein, S. A., and Reindl, D. T., 2007, A finite-time thermodynamic framework for optimizing solar-thermal power plants, Journal of Solar Energy Engineering, 129(4), pp. 355–362.

Michel, Y., Haller, C.A., Cruickshank, W.S., Harrison, S.J., Andersen, E., Furbo, S., 2009, Methods to determine stratification efficiency of thermal energy storage processes – Review and theoretical comparison, Solar Energy, Vol. 83, Issue 10, October 2009, pp. 1847-1860.

Montes, M.J., Abánades, A., Martínez-Val, J.M., and Valdés, M., 2009, Solar multiple optimization for a solar-only thermal power plant, using oil as heat transfer fluid in the parabolic trough collectors, Solar Energy, Vol. 83 (12), Dec. 2009, pp. 2165-2176.

Nassar, Y., ElNoaman, A., Abutaima, A., Yousif, A., Salem, A., 2006, Evaluation of the underground soil thermal storage properties in Libya, Renewable Energy, Volume 31, Issue 5, April 2006, Pages 593-598.

Nellis, G., and Klein, S., 2009, *Heat Transfer,* Cambridge University Press.

Pacheco, J.E., Showalter, S.K., and Kolb, W.J., 2002, Development of a molten salt thermocline thermal storage system for parabolic trough plants, Journal of Solar Energy Engineering, 124(2), pp. 153–159.

Pitz-Paal, R., Dersch, J., Milow, B., Tellez, F., Ferriere, A., Langnickel, U., Steinfeld, A., Karni, J., Zarza, E., Popel, O., 2007, Development steps for parabolic trough solar power technologies with maximum impact on cost reduction, Journal of Solar Energy Engineering, 131, pp. 371-377.

Polyanin, A. D., 2002, *Handbook of Linear Partial Differential Equations for Engineers and Scientists*, Boca Raton: Chapman & Hall/CRC Press, ISBN 1-58488-299-9.

Price, H., Lupfert, E., Kearney, D., Zarza, E., Cohen, G., Gee, R., Mahoney, R., 2002, Advances in parabolic trough solar power technology, Journal of Solar Energy Engineering, Vol. 124, May 2002, pp. 109-125.

Product Resources, http://www.radcoind.com/index.html

Regin, A. F., Solanki, S.C., Saini, J.S., 2008, Heat transfer characteristics of thermal energy storage system using PCM capsules: A review, Renewable and Sustainable Energy Reviews 12 (2008) 2438–2458.

Renewables 2007, 2008, Global Status Report, Issued by Renewable Energy Policy Network for the 21st Century (www.REN21.net).

Reuss, M., Beck, M., Muller, J.P., 1997, Design of a seasonal thermal energy storage in the ground, Solar Energy, Vol. 59, No. 4-6, April-June 1997, pp. 247-257.

Sari, A., Kaygusuz, K., 2001, Thermal performance of myristic acid as a phase change material for energy storage, application. Renewable Energy, 24 (2001) 303–317.

Schumann, T. E.W., 1929, Heat transfer: a liquid flowing through a porous prism. Journal of the Franklin Institute, 208(3), pp. 405 – 416.

Shitzer, A., and Levy, M., 1983, Transient behavior of a rock-bed thermal storage system subjected to variable inlet air temperatures: Analysis and experimentation. *Journal of Solar Energy Engineering,* 105(2), May, pp. 200–206.

Singer, C., Buck, R., Pitz-Paal, R., and Müller-Steinhagen, H., 2010, Assessment of solar power tower driven ultrasupercritical steam cycles applying tubular central receivers with varied heat transfer media. Journal of Solar Energy Engineering, 132, 041010.

Spiers, D.J., and Rasinkoski, A.D., 1995, Predicting the service lifetime of lead/acid batteries in photovoltaic systems, J. Power Sources, vol. 53, no. 2, pp. 245–253.

Therminol VP-1 heat transfer fluid by Solutia, 1999, Technical Bulletin 7239115B, Solutia, Inc., 1999.

Tritt T.M., 2005, Thermal Conductivity: Theory, Properties, and Applications (Physics of Solids and Liquids), Springer, 2005-05-13, ISBN: 0306483270.

Van Lew, J.T., Li, P.W., Chan, C.L., Karaki, W., Stephens, J., 2009, Transient heat delivery and storage process in a thermocline heat storage system, IMECE2009-11701, Proceedings of the ASME 2009 International Mechanical Congress and Exposition, November 13-19, 2009, Lake Buena Vista, Florida, USA.

Van Lew, J.T., Li, P.W., Chan, C.L., Karaki, W., Stephens, J., 2011, Analysis of heat storage and delivery of a thermocline tank having solid filler material, Journal of Solar Energy Engineering, MAY 2011, Vol. 133/021003.

Wu, S.M., Fang, G.Y., Liu, X. 2011, Dynamic discharging characteristics simulation on solar heat storage system with spherical capsules using paraffin as heat storage material, Renewable Energy, 36 (2011) 1190-1195.

Wyman, C., Castle, J., Kreith, F., 1980, A review of collector and energy storage technology for intermediate temperature applications, Solar Energy, Vol. 24, No. 6, 1980, pp. 517-540.

Yang, Z., Garimella, S.v., 2010, Molten-salt thermal energy storage in thermoclines under different environmental boundary conditions, Applied Energy, Vol. 87, No. 11, November 2010, pp. 3322-3329.

Zalba, B., Marin, J.M., Cabeza, L.F., Mehling, H., 2003, Review on thermal energy storage with phase change: materials, heat transfer analysis and applications, Applied Thermal Engineering, 23 (2003) 251–283.

Zarty, O., Juddaimi, A. E., 1987, Computational models of a rock-bed thermal storage unit, Solar and wind Technology, 2(4), pp. 215- 218.

Zhang, D., Li, Z.J., Zhou, J.M., Wu, K.R., 2004, Development of thermal energy storage concrete , Cement and Concrete Research, Vol. 34, No. 6, June 2004, pp. 927-934.

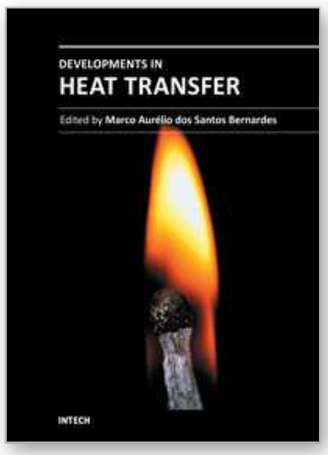

Developments in Heat Transfer

Edited by Dr. Marco Aurelio Dos Santos Bernardes

ISBN 978-953-307-569-3
Hard cover, 688 pages
Publisher InTech
Published online 15, September, 2011
Published in print edition September, 2011

This book comprises heat transfer fundamental concepts and modes (specifically conduction, convection and radiation), bioheat, entransy theory development, micro heat transfer, high temperature applications, turbulent shear flows, mass transfer, heat pipes, design optimization, medical therapies, fiber-optics, heat transfer in surfactant solutions, landmine detection, heat exchangers, radiant floor, packed bed thermal storage systems, inverse space marching method, heat transfer in short slot ducts, freezing an drying mechanisms, variable property effects in heat transfer, heat transfer in electronics and process industries, fission-track thermochronology, combustion, heat transfer in liquid metal flows, human comfort in underground mining, heat transfer on electrical discharge machining and mixing convection. The experimental and theoretical investigations, assessment and enhancement techniques illustrated here aspire to be useful for many researchers, scientists, engineers and graduate students.

INTECH
open science | open minds

InTech Europe
University Campus STeP Ri
Slavka Krautzeka 83/A
51000 Rijeka, Croatia
Phone: +385 (51) 770 447
Fax: +385 (51) 686 166
www.intechopen.com

InTech China
Unit 405, Office Block, Hotel Equatorial Shanghai
No.65, Yan An Road (West), Shanghai, 200040, China
中国上海市延安西路65号上海国际贵都大饭店办公楼405单元
Phone: +86-21-62489820
Fax: +86-21-62489821

IntechOpen